Review Article

Liquid metals nanotransformer for healthcare biosensors

Yunlong Bai[1,2,#], **Jie Zhang**[1,3,#], **Chennan Lu**[1,3,#], **Wei Rao**[1,3,*] iD

[1]Technical Institute of Physics and Chemistry, Chinese Academy of Sciences, Beijing 100190, China.
[2]School of Engineering Science, University of Chinese Academy of Sciences, Beijing 101408, China.
[3]School of Future Technology, University of Chinese Academy of Sciences, Beijing 101408, China.
[#]Authors contributed equally.

[*]**Correspondence to:** Prof. Wei Rao, Technical Institute of Physics and Chemistry, Chinese Academy of Sciences, No.29 Zhongguancun East Road, Beijing 100190, China. E-mail: weirao@mail.ipc.ac.cn

Abstract

Featuring low cost, low melting points, excellent biocompatibility, outstanding electrical conductivity, and mechanical properties, gallium-based liquid metals (LMs) have become a promising class of materials to fabricate flexible healthcare sensors. However, the extremely high surface tension hinders their manipulation and cooperation with substrates. To address this problem, the inspiration of nanomaterials has been adopted to mold LMs into LM nanoparticles (LMNPs) with expanded advantages. The transformability of LMNPs endows them with functionalities for sensors in multiple dimensions, such as intelligent response to specific molecules or strains, various morphologies, integration into high-resolution circuits, and conductive elastomers. This review aims to summarize the superior properties of LMs, transformability of LMNPs, and correlated advantages for sensor performance. Multidimensional functional sensing forms consisting of LMNPs and corresponding applications as healthcare sensors will be presented. In the end, the existing challenges and prospects in the processing and application of LMNPs will also be discussed.

Keywords: Liquid metal, nanoparticles, transformability, healthcare biosensors, flexible electronics

INTRODUCTION

Sensors usually convert the stimuli received into optical, electrical, magnetic, and other signals, eventually

transmitting to the receiving end in the form of optical[1] or electrical signals. In the field of health care sensors, the physiological signals of the human body include muscle movement, metabolic fever, cardiac electrical signals, electromyographic (EMG) signals, urine, sweat, *etc.* The combination of these physiological signals will indicate the state of health, and the long-term data collection through the sensors will facilitate health monitoring and disease diagnosis, thus enabling early intervention in disease treatment[2]. This asks for functional stability and structural durability for materials. In addition, the impact of the environment on human health should not be underestimated. Exposure to ambient noise, low air pressure, hazardous gases, or unsuitable temperatures for a prolonged period can be harmful to humans, so sensors are also needed to detect environmental information in real time.

However, due to the non-planar shape of the human body and frequent body movements, traditional rigid sensors can no longer cope with such complex working conditions[3]. Therefore, flexible and electrically conductive materials need to be introduced to overcome this disadvantage. The sensor mainly comprises a flexible substrate and a conductive material filling the substrate[4]. The flexible substrate can ensure a close fit between the sensor and the body, while the flexibility allows the sensor to bend and stretch with muscles. However, the common flexible substrate materials [polydimethylsiloxane (PDMS)[5-12], polyimide[13-18], Ecoflex[19-21], polyurethane (PU)[22-25], and poly(vinyl alcohol) (PVA)[26-28]] are usually electrically insulating, so they need to be filled with conductive material to form a conductive path to realize signal transmission. The universal filler materials are metal nanoparticles (NPs)[8,29-32], metal nanowires[33], and carbon-based nanomaterials, such as carbon nanotubes (CNT)[12,20,23,30,34,35], graphene[11,13,36,37], and carbon black[8,38]. However, limited by the cost or inherent mechanical property defects, applying the above materials in flexible sensors requires structure design and mechanical match. Gallium-based LMs have excellent thermal and electrical conductivity[39-43] and find applications in energy[44,45] and soft robotics[46,47] applications. Therefore, they are used as filler materials. LMs also exhibit excellent flexibility and stretchability[39,40], reducing damage to the substrate and ensuring that the electrical conductivity of materials remains stable during the stretching process. Gallium-based LMs are less harmful to biological tissue and, therefore, could be used in dentistry as an alternative to mercury[48], indicating outstanding biocompatibility[49,50]. The rich surface properties, including the chemical properties of the oxide film[49,51,52] and the controlled composition of the oxide film[53], also allow for multiple forms of conversion of the sensing signal. Nevertheless, when macro LMs are fabricated into composites and wrapped, leakage is difficult to avoid[54], and direct-written LM circuits have poor adhesion[55]. Microfluidic sensors have relatively complex fabrication processes[56], and their integration can be challenging. Fortunately, by exploiting the liquid deformability of LMs, it is possible to prepare macroscopic LM droplets down to the nanoscale using methods such as ultrasonics, *etc.*[57-59] The resulting LMNPs not only have the basic properties of macroscopic LM droplets but also have a higher specific surface area, thus giving the LM more reaction area[60]. Additionally, they have properties such as self-healing[61] and plasmon resonance. The filling of LMNPs into flexible substrates can reduce the leakage of LM to a certain extent while simplifying the preparation process compared to microfluidic sensors.

Based on the information presented above, the application of transformable nano-LM sensors for human health detection appears to be essential, and therefore, this paper aims to present the progress of research on this sensor in the field of life and healthcare monitoring. The physical and chemical properties involved in the use of LMs as sensor materials are presented, followed by a comparison of the unique transformable properties of LMs for sensor applications, and then the main structures of existing nano-LM sensors are discussed. Finally, the latest research and applications of nano-LM flexible sensors in human health and the development of nano-LM sensors are also introduced [Figure 1].
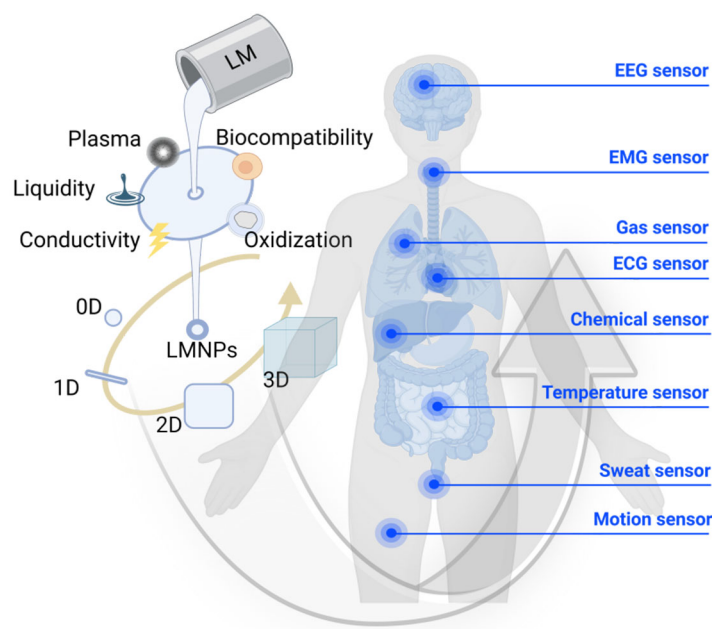
Figure 1. Properties, constructions, and applications of LM nanotransformers for healthcare biosensor. ECG: Electrocardiographic; EEG: electroencephalographic; EMG: electromyographic; LM: liquid metal; LMNPs: LM nanoparticles.

BASIC PROPERTIES OF LMS FOR SENSORS

Basic properties of gallium-based LMs

Low melting point and liquid nature

Compared to rigid materials, substances in the liquid phase can be prepared in a more straightforward way to obtain micro and nanoscale particles or droplets, which is largely owing to the lower energy required to shear the liquid[62]. As shown in Table 1[51,63-72], gallium-based LMs are a series of alloys formed by gallium and other metals, such as In, Sn, Zn, *etc.* The melting point of gallium-based LMs is lower than room temperature and varies with the type and number of metals added, with the general rule being that the more metals added, the lower the melting point and that the wide liquid temperature range allows the LMs to operate in a range of temperature zones that includes the normal temperature range of the human body. Also, similar to water, LMs have unusual spatial ductility, which will facilitate the preparation of high-quality flexible sensor devices from LMs. For example, in contrast to the "flexibility" exhibited by ordinary metals made into foil, LMs can be spatially stretched and compressed at any angle and without internal stress or mechanical damage to the substrate, whereas metal foils can only be spatially deformed in one dimension and to a limited extent[73,74]. However, the surface tension of LMs is extremely high, about ten times that of water, making them often behave in a spherical form in solutions such as NaOH. The high surface tension implies a low wettability, which means that it is difficult for LMs to adhere directly to the surface of a substrate. Yet, when LM is exposed to air, it is straightforward to produce a thin layer of oxide film, which will reduce the surface tension of the droplet[63]. In order to improve the performance defects caused by the high surface tension of macroscopic LMs, some researchers have used electrical potential to regulate the surface tension of the material[75]; others have found that adding certain metal particles (Cu[76], Ni[40,77], Fe[78]) or inorganic materials (Mxene[79], SiO_2[80]) to a LM can also reduce its surface tension, and another idea is to prepare macroscopic LMs to nano size[63], the property of LMNP suspension, such as surface tension and viscosity, is dominated by solvents instead of LMs. LMNPs behave more akin to solid particles because of the existence of surface oxide films, even though the interior part is still liquid at room temperature.

Table 1. Physical properties of classic filling materials

Material	Density (g/cm³)	Melting point (°C)	Surface tension (mN/m)	Conductivity 10⁶ (S/m)
Ga	5.91 (25 °C)[c]	29.8[c]	711 (30 °C)[a]	7.4 (25 °C)[c]
In	7.31 (25 °C)[c]	157[c]	556 (157 °C)[a]	12.5 (25 °C)[c]
Ag	10.5[e]	961[h]	-	60.6 (26.5 °C)[b]
Cu	8.9[g]	1,084[a]	-	58 (26.5 °C)[b]
Au	19.3[e]	1,064[f]	-	44 (26.5 °C)[b]
EGaln ($Ga_{75}In_{25}$)	6.28 (20 °C)[c]	15.5[b]	624[d]	3.4 (22 °C)[c]
Galinstan ($Ga_{68.5}In_{21.5}Sn_{10}$)	6.44 (20 °C)[c]	10.5[b]	600[b]	3.5 (20 °C)[c]
$Ga_{61}In_{25}Sn_{13}Zn_1$	6.5[k]	7.6[k]	500[k]	2.8[k]
CNT	0.5-3.5[i,*]	-	-	0.001-10[i,#]
Water	1.0[j]	0[j]	72.8 (25 °C)[j]	-

[a]Data from[51]; [b]Data from[63]; [c]Data from[64]; [d]Data from[65]; [e]Data from[66]; [f]Data from[67]; [g]Data from[68]; [h]Data from[69]; [i]Data from[70]; [j]Data from[71]; [k]Data from[72]; [*]The density of the CNT is influenced by factors such as their diameter, the number of biscuits, *etc.*; [#]The conductivity of CNTs is influenced by factors such as their diameter, fabrication processes, and alignment. The letter in the upper right corner of the data indicates the cited literature in the reference column. CNT: Carbon nanotubes.

Electrical conductivity

The conductivity of the sensing material has a significant impact on the performance of the sensor. High conductivity will help to form a good correlation between external stress and changes in the electrical properties of the material to improve the sensitivity and linearity of the sensor. Excellent electrical conductivity is one of the key reasons why LM materials are widely used in the sensor field. Based on the liquid state and high electrical conductivity of LMs, it is possible to form a low-resistance conductive path in an insulating matrix. As shown in Table 1, certain rigid metals, such as gold, silver, and copper[63], have an intrinsic conductivity that is 6-8 times higher than those of LMs, but their higher cost and rigid characteristic limits their widespread use in the flexible and stretchable sensor. On the other hand, carbon-based materials generally have lower conductivities than those of LMs, making LMs an important candidate for conductive filler materials for flexible sensors. Furthermore, by mixing highly conductive particles (Cu, Ag) with LMs, the conductivity of LMs can be enhanced even more. For example, the oxidation film of Cu particles and eutectic gallium-indium alloy (EGaIn) is removed in the presence of an alkaline solution and electrical potential, and the conductivity of the mutually doped material is 1.8 times higher than that of pure EGaIn[76]. This method also allows the configuration of materials with different Cu contents, offering enhanced conductivity potential for LMs.

Gallium-based oxide layer

Exposure of LMs to air results in the formation of an amorphous oxide film (Ga_2O_3) on the surface of droplets. Among many structures, β-Ga_2O_3 is the most thermodynamically stable[81]. On the one hand, the oxide film passivates to protect the LM inside while preventing droplet aggregation and facilitating the formation and stable existence of NPs. On the other hand, Ga_2O_3 has an intrinsic n-type conductivity[82], and its conductivity depends mainly on the carrier concentration and electron mobility of the material[83], both of which would change when Ga_2O_3 is exposed to the target gas, causing changes in Ga_2O_3 conductivity or resistance, so Ga_2O_3 can be used in gas detection sensors. The mechanisms by which Ga_2O_3 detects target gases can be divided into three categories, with different mechanisms dominating at different temperatures[84] as follows: (i) At high temperatures, the ambient oxygen concentration and Ga_2O_3 oxygen concentration are in dynamic equilibrium, when the ambient oxygen concentration decreases, the concentration of positively ionized oxygen defects within Ga_2O_3 increases and its delocalized electrons increase, leading to an increase in the conductivity of the material; (ii) When the temperature drops, reducing gases, such as CH_4, will attach to the crystal surface and react with Ga_2O_3, which will release conduction electrons within the material and increase its conductivity; (iii) When the temperature is lower,

the reducing gases will be more beneficial to the grain boundaries for electron transport, leading to an increase in conductivity.

Optical induction

The optical property of LMNPs opens the door to optical sensing, the most important of which is the localized surface plasmon resonance (LSPR) phenomenon. When noble metal NPs are irradiated by light matching their vibrational frequencies, they will produce a strong absorption of photon energy and result in LSPR[85]. As a broadband plasmonic material, Ga has a plasmon frequency similar to Al with a bulk plasmon energy of up to 14 eV, making Ga an ideal material for achieving LSPR in the ultraviolet (UV) region[1,86]. It has been shown that the metal oxide (MO) layer on the surface of Ga NPs can increase the mechanical and chemical stability[87,88], and the effect of the optical phenomenon of LSPR can be controlled by adjusting the particle diameter[89], particle coupling[87] and altering the MO layer[86]. Moreover, surface-enhanced Raman scattering based on LSPR is also feasible and can be achieved by LSPR-enhanced inelastic light scattering[90,91]. In addition, some important optical phenomena are worth noting. For example, the dipole modes of GaNPs can be tuned with the range of spectral regions[92]. The electric coupling substitution reaction can visualize the chemistry of GaNPs preparation as an optical tuning phenomenon of the LSPR in the UV region[93], and the temperature change can be indicated by the change of extinction cross section at the resonance through the solid-core/liquid-shell structure of LMNPs[1,94]. Research on Ga NP fluorescence[95], Raman-enhanced Ga plasmon[96-98], and deposited optically responsive materials[99] is now in full swing, which has led to Ga applications in optical sensors being successfully transformed into a popular research topic, such as surface plasmon resonance biosensors[100], surface-enhanced Raman scattering sensors[90,101,102], and photoluminescent biosensors[99,103].

Biocompatibility

Many sensors are in direct contact with living organisms and should not endanger biological health, so it is necessary and vital to discuss the biocompatibility of LMs. Typically, macroscopic gallium-based LMs have been applied to teeth, nerves, and bones as repair materials[104,105]. Because the vapor pressure on the surface of gallium is negligible at room temperature and almost non-volatile, there is no pathogenic potential from volatilization and inhalation, as seen with mercury. Also, gallium and its alloys are non-corrosive and non-permeable for direct contact with living organisms[106]. However, gallium-based LMNPs do not have precisely the same properties as macroscopic alloys. Due to their small particle size, LMNPs can be transported to organs and tissues of living organisms via the reticuloendothelial system with blood[106-108]. Theoretically, the smaller the volume, the larger the specific surface area and the higher the solubility, while the reaction of gallium with water produces hydroxy gallium oxide[109,110], which may lead to the imbalance of reactive oxygen species[109,111]. Also, the further hydrolytic ionization of hydroxy gallium oxide produces free gallium ions[109,110], which may pose a burden risk to organs such as the kidney, liver, and brain of organisms[112]. For example, Schedle *et al.* experimentally found that DNA fragments of murine HL-60 cells were detected to be broken after incubation in Ga^{3+} environment at 1 mmol/L for 6 or 72 h, and for L-929 ^{3}H-thymidine, incorporation of fibroblasts was inhibited at Ga^{3+} concentrations greater than 0.033 mmol/L[113], suggesting that toxicity is directly linked to dose and that larger doses of LMNPs may lead to increased organ burden. However, in most biological experiments, the toxicity of LMNPs was not manifested, probably due to the low concentration of LMNPs required for the investigation.

At the cellular level, Chechetka *et al.* tested cell viability after treatment with different concentrations of LMNPs and other nanomaterials, such as multi-walled CNTs (MWCNTs), single-walled CNTs, and gold nanorods. LMNPs were found to have a higher survival rate than other nanomaterials under the same experimental conditions, and the advantage increased significantly with increasing concentrations over the testing range [Figure 2A i][114]; Tang *et al.* investigated the effect of surface modification on LMNPs toxicity.
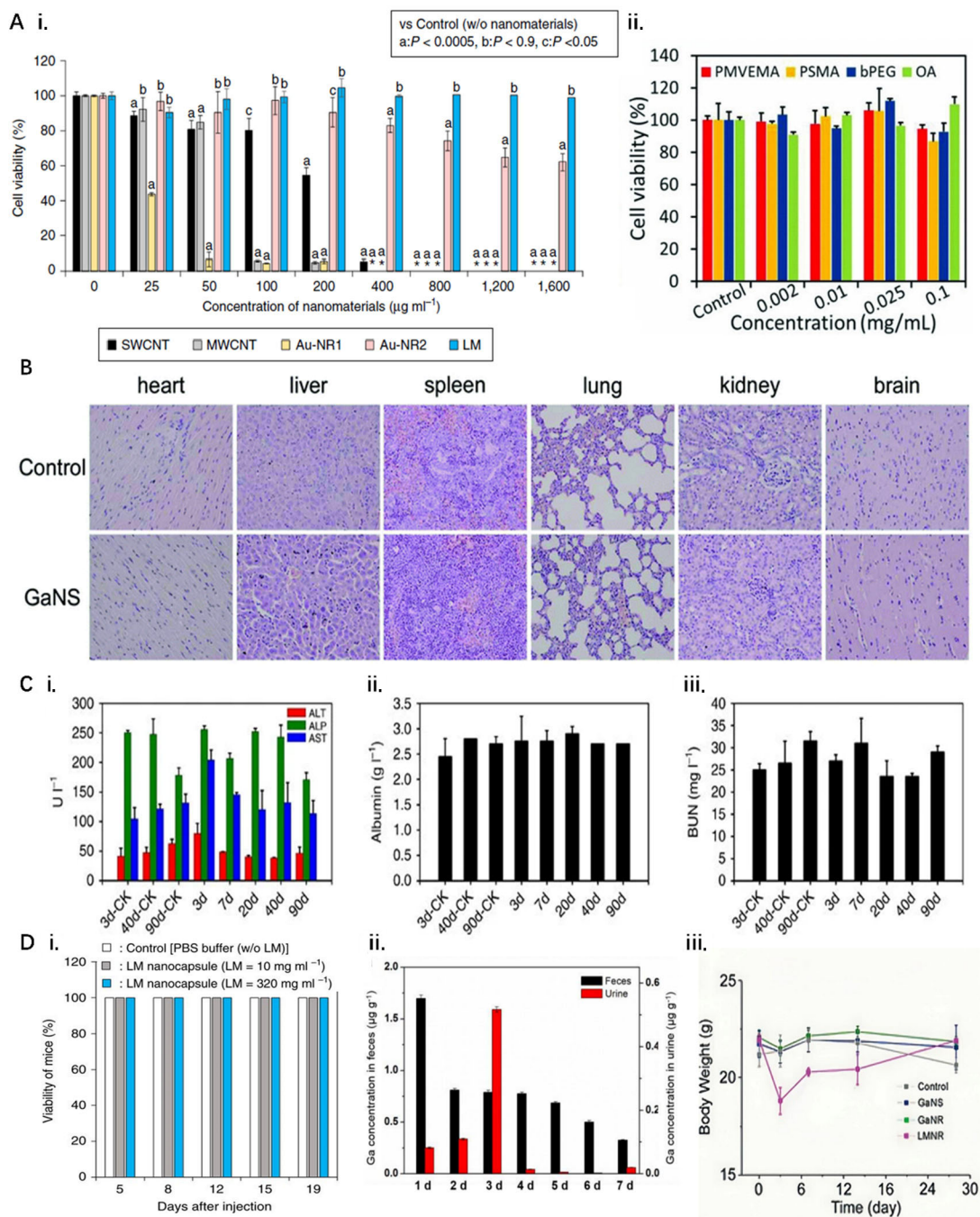
Figure 2. Biocompatibility assay of LMNPs. (A) Cellular level. (i) Survival under different nanomaterials in culture[114], *symbols indicate all cells died; (ii) Survival of MCF-7 cells cultured at different concentrations of molecularly grafted LMNPs[115]; (B) Tissue level. Histological characterization of impact of LMNPs to major organs[116]; (C) Organ level. Liver function indicators in mice after injection of 45 mg·kg^{-1} LMNPs[117]. (i) ALT, ALP, and AST levels; (ii) albumin concentrations; and (iii) BUN measured at different times in LM-NP/L blood; (D) Biological level. (i) Survival of mice injected with LMNPs over time[114]; (ii) Determination of gallium in stool and urine of mice after injection of LMNPs[117]; (iii) Changes in body weight of mice after injection of different types of LMNPs[116]. ALP: Alkaline phosphatase; ALT: alanine aminotransferase; AST: aspartate aminotransferase; bPEG: brushed polyethylene glycol; BUN: blood urea nitrogen; LM: liquid metal; LMNPs: LM nanoparticles; MWCNT: multi-walled carbon nanotube; OA: oleic acid; PMVEMA: poly methyl vinyl ether-alt-maleic anhydride; PSMA: poly styrene-co-maleic anhydride.

The results of Alamar Blue experiments showed that the survival of MCF-7 cells under the conditions of

LMNPs grafted with different molecules was up to 90% or even more than 100% [Figure 2A ii][115].

At the tissue level, Sun *et al.* administered LMNPs intravenously to mice and performed H&E stained images of several tissue sites, including heart, liver, spleen, lung, kidney, and brain; after photothermal treatment and execution of the mice, no significant tissue damage was detected [Figure 2B][116].

At the organ level, Lu *et al.* explored the effects of LMNPs on major liver function indicators, including alanine aminotransferase (ALT), aspartate aminotransferase (AST), alkaline phosphatase (ALP), albumin concentrations, and blood urea nitrogen (BUN), which remained largely unchanged after intravenous administration, suggesting no substantial toxicity of LMNPs [Figure 2C][117].

At the living organisms level, Chechetka *et al.* found that all five mice survived normally for 19 days after being injected with LMNPs [Figure 2D i][114]. Lu *et al.* suggested that the mice may have cleared the injected LMNPs through their feces and liver and excreted them [Figure 2D ii][117]. Meanwhile, Sun *et al.* conducted *in vivo* experiments on different forms of LMNPs, among which gallium nanorods and gallium nanospheres did not reveal any abnormalities in body weight and blood tests in mice in the experimental concentration range [Figure 2D iii][116]; however, for gallium-indium alloy nanorods (LMNR) containing indium, mice showed weight loss on the third day, and abnormally high white blood cell data up to about 300% were found starting on the seventh day[116]. This indicates that excess indium ions are enriched in organisms for long periods of time and may pose a potential threat to the health of organisms. Further illustrating LMNPs of other elements, indium NPs do not release indium ions under static conditions in water while applying ultrasound stimulation rapidly increases indium ion concentration[106,118], and excessive concentrations of indium ions have now been shown to cause physical weakness, weight loss, liver and spleen lesions, and more in humans[119].

In conclusion, gallium-based LMNPs have been widely used in biomedical research, such as drug delivery, medical imaging, and cancer therapy[114,120,121] due to acceptable low toxicity. However, when LMNPs are injected into organisms, especially in large quantities or accompanied by subsequent operations such as ultrasound and laser, the metabolism of metal ions, such as gallium and indium ions, by the organisms should be monitored in a timely manner and a comprehensive long-term biological health testing to ensure the stability and safety of biomaterials.

PREPARATION OF NANO-LMS

As is commonly known, the current approaches can be divided into bottom-up and top-down ideas according to the idea of preparing NPs[122]. For LMs, bottom-up approaches mainly include physical vapor deposition[123] and thermal decomposition[124], which allow for the controlled size distribution of NPs. However, the preparation processes are more complex compared to top-down approaches. Given the excellent deformability of LMs, top-down preparation of NPs has become a more widely accepted method, with ultrasonic preparation and mechanical shearing being the two dominant approaches for large-scale fabrication, which will be introduced in the following.

Ultrasonication

Ultrasonication is widely used to prepare LM nanomaterials as a top-down strategy. The ultrasonic probe vibrates to arouse microbubbles and cavities within the solvent, generating localized high temperature and pressure, which strongly shatter the bulk LM into smaller droplets[112,125] [Figure 3A]. The eventual mean size and morphology of LMNPs are influenced by various factors such as the frequency and duration of the applied ultrasound[125,126], the type of solvent used for the sonication[125], and the temperature during
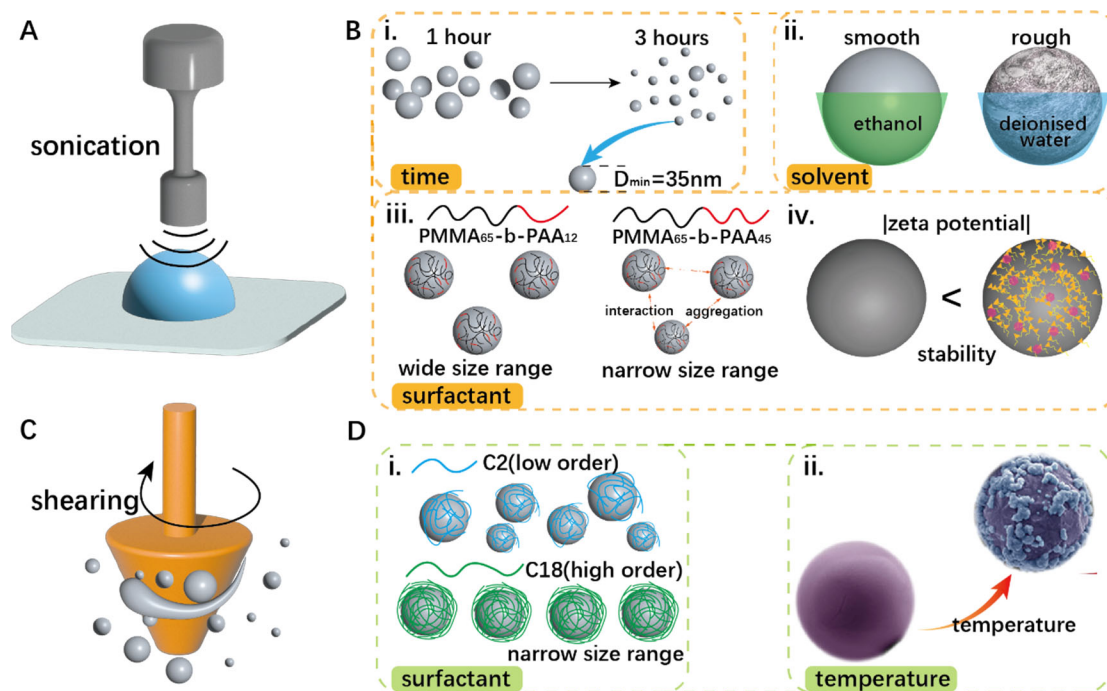
Figure 3. Preparation of nano-LMs. (A) Schematic diagram of LMNPs prepared by ultrasound; (B) Influencing factors of ultrasonic preparation of LMNPs. (i) Changes in size distribution of LMNPs with time; (ii) Surface properties of LMNPs in different solvents; (iii) Surfactants affect the particle size distribution of LMNPs; (iv) Surfactants improve stability of LMNPs solutions; (C) Schematic diagram of the preparation of nano-LMs by shearing; (D) Factors affecting shear preparation of LMNPs. (i) Surfactants affect the particle size distribution of LMNPs; (ii) Temperature-induced changes in the composition of LMNPs[144]. LMs: Liquid metals; LMNPs: LM nanoparticles.

sonication[126,127]. For example, during the initial stage, as time progresses, the size of the NPs becomes smaller, and their size distribution becomes more concentrated[125] [Figure 3B i]. However, it has been shown that the size of LMNPs does not always decrease with sonication time but eventually stabilizes around a specific size range[126] [Figure 3B i]. On the other hand, higher ultrasonic frequencies and lower temperatures will help to produce smaller droplets. In addition, the surface of the NPs is very rough when the LM is sonicated in deionized water, whereas the surface of the LM is smoother when sonicated in ethanol and hexane [Figure 3B ii], which is mainly influenced by the gallium oxide hydroxide (GaOOH) crystal[125].

Over time, LMNPs in solvents are gradually deposited by gravity[128]; therefore, surfactants need to be added in order to allow the NPs to be uniformly distributed in the solvent. Common surfactants are thiol-based surfactants, brushed polyethylene glycol[129], poly(1-octadecene-alt-maleic anhydride)[130], and 2-amino-2-(hydroxymethyl)-1,3- propanediol[131]. Furthermore, studies have shown that surfactants also influence the preparation of NPs; for example, $C_{18}H_{37}$-SH was shown to not only stabilize LMNPs but also increase the yield of NPs[132], while poly(methyl methacrylate)-block-poly(acrylic acid) (PMMA-b-PAA) was found to lead to different size distributions of NPs for various degrees of polymerization of PAA[133] [Figure 3B iii]. The potential difference between the slipping plane of the NPs and the solvent is known as the zeta potential[134]. A high zeta potential means that the particles are more charged compared to their environment. Therefore, the higher the absolute value of the zeta potential, the more stable the colloidal solution[135]. Surfactant coverage causes changes in the zeta potential of the composite particles[136-138] [Figure 3B iv], so measuring the change in the zeta potential of the colloidal solution can determine whether the surfactants cover the particle surfaces and whether the NPs are stably distributed within the colloid. Not

to be overlooked, surfactants also provide a steric barrier to the system to maintain colloidal stability, where they also play a key role in many solutions[130,139].

Mechanical shearing

Mechanical shearing is a straightforward preparation process in which a velocity and pressure difference is created in the solution by rotating the tool so that the LM is subjected to centrifugal, shear, and tensile forces, plus the gravity of the LM itself [Figure 3C][140]. Under the forces applied, the droplet shears into two smaller droplets when the droplet deformation exceeds a certain limit (Rayleigh-Plateau limit). By controlling the rotational speed and choosing the right solution (to obtain different shear forces), droplets of various sizes can be obtained. Surfactants are also essential for the stability of the NPs during the preparation process; some used in the study are acetic[140,141], chitosan[142], and carboxylic acids[143]. As part of the solution, the surfactant influences the size and morphology of the NPs [Figure 3D i]. In the case of carboxylic acid, for example, the NPs prepared from surfactants with hydrocarbon chain lengths of eight (C8) and below show a broad size distribution, while C16 and above show a more concentrated distribution, which is mainly due to the ordered nature of the chains[143] [Figure 3D i]. In addition, temperature can also affect the morphology of the NPs; taking EGaIn as an example, by increasing the temperature, the thickness of the gallium oxide film can be improved while creating a chemical gradient. When the temperature rises to a certain value, the gallium oxide film will break down and cause the internal indium-rich fluid to leak out and form an indium oxide layer on the surface [Figure 3D ii], resulting in a compositional inversion[144].

TRANSFORMATION OF LMS IN SENSORS
Physical transformation
Particle sintering

Since the oxide layer on the surface of LMNP is a poor electrical conductor, it is hard to form an effective conductive path between droplets in sensors. External stimuli are required to break the oxide film so that the composite can be converted from a dielectric to a conductive state[145]; this process is known as "sintering" [Figure 4A i and ii]. Compared to the sintering method of conventional nanoscale metallic particles, LM can, by virtue of its liquid nature, rupture the rigid oxide film after being subjected to minor applied stress, resulting in the LM spilling out and thus forming a circuit[146], as shown in Figure 4A i and ii. This mechanical sintering method is unique to LMNPs, and compared to the sintering methods of conventional nanometal particle sensors, such as laser sintering and high-temperature sintering[147], the operation is simple and economical. In addition, the metals that make up conventional nanometal sensors, such as Ag nanowires, have high contact resistance with each other and require high-temperature sintering or point-to-point sintering[148], and similarly, copper particles are sintered with attention to the uniformity of the connection of the particle necking[149], while LMs are subject to either mechanical stress (mechanical sintering) or thermal stress from the difference in thermal expansion inside and outside the droplet (laser sintering or thermal sintering), the LM inside the droplet will be completely mixed after the destruction of the oxide film, forming a circuit without contact resistance, thus achieving lower energy consumption.

Sensing information detection and acquisition

LMNP-filled materials can be used as sensor materials because the low Young's modulus of LMs makes them extremely sensitive to external stresses[150]. When the substrate is deformed by the applied stresses, the LM will also accordingly deform, inducing changes in the cross-sectional area, conductive paths, and number of contact sites[151], thus causing changes in the electrical signal of the monitoring circuit [Figure 4A iii]. In contrast to conventional rigid-filled materials, where changes in sensing signals such as resistance are achieved by the fracture of the substrate when subjected to tension[152,153], the deformation mechanism of the LM causes minimal damage to the substrate and is nearly fully compliant[154].
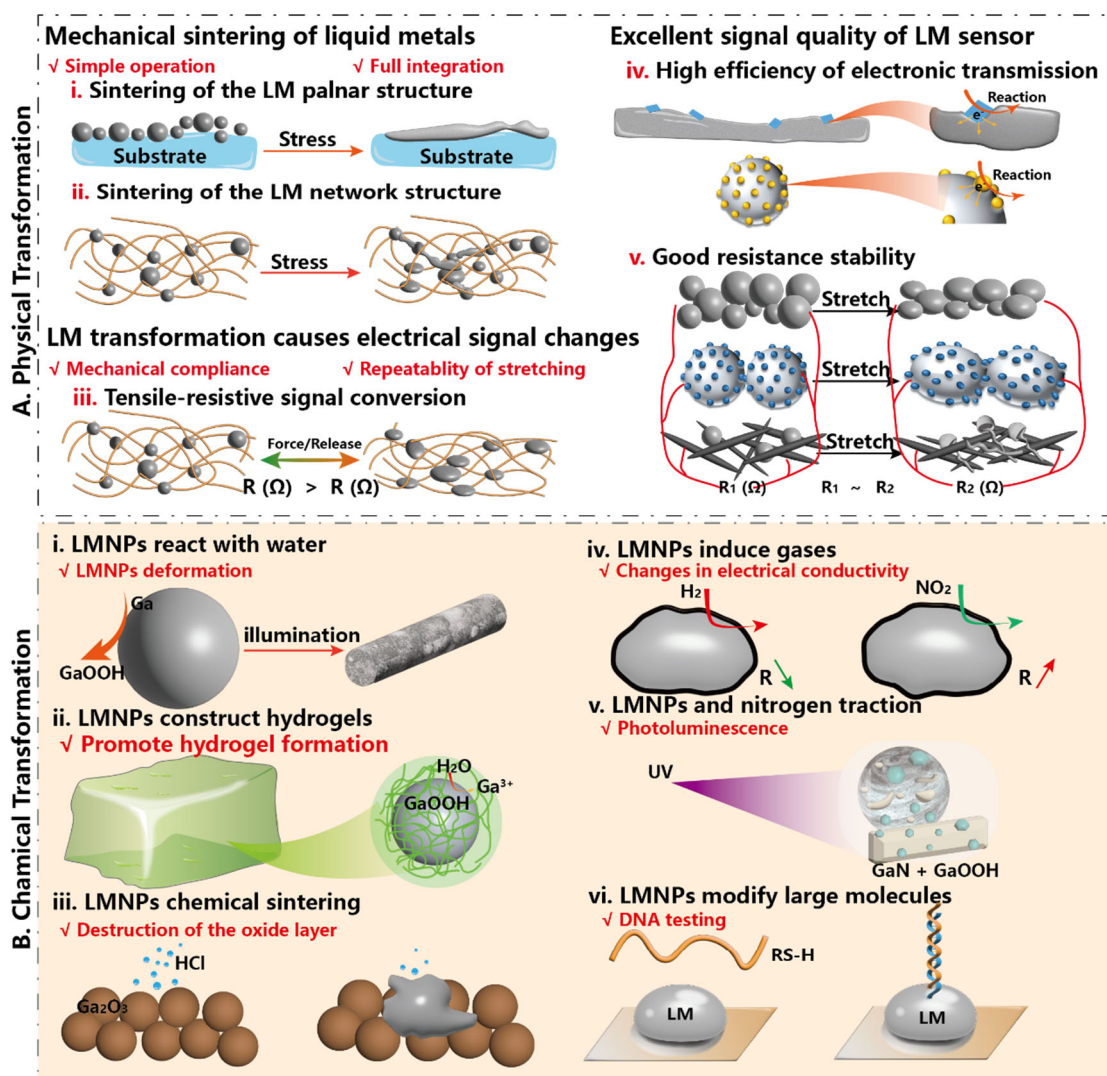
Figure 4. Transformation of LMs in sensors' fabrication and function. (A) Physical transformation: (i) and (ii) Sintering of LMs with different structures; (iii) Generating electrical signal changes using LMs transformation; (iv) Excellent resistance stability of LM materials during transformation; (v) Low resistance to charge transfer due to interface contact; (B) Chemical transformation: (i) Reaction of Ga with H_2O and photodeformation of LMNPs; (ii) Reaction of GaOOH with H_2O to prepare hydrogels; (iii) Reaction of Ga_2O_3 with HCl for chemical sintering; (iv) Ga_2O_3 reacts with H_2 for enhanced electrical conductivity; (v) Ga reacts with N_2 to give LMNPs photoluminescent properties; (vi) Ga reacts with RS-H to give LMNPs the ability to detect specific DNA. LM: Liquid metal; LMNPs: LM nanoparticles.

Sensing information transmission

The information transfer capability of a sensor can be evaluated in a number of dimensions, such as the sensitivity of the received information and the long-term cycling stability of the resistors. The efficiency of charge transfer has a significant impact on the sensitivity of a sensor, and LMs are both flexible and highly conductive, allowing them to conform to the shape of the material to create good interfacial contact and provide more transfer channels, thus reducing the impediment to charge transfer between different substances [Figure 4A iv]. For example, the two-dimensional material SnS_2 is often used to prepare sensors to detect the presence and content of certain types of gases as it reacts to gas stimuli by transferring and transferring charge and causing a change in the electrical signal, and when SnS_2 is in contact with a sintered LM electrode, the good charge flow results in a linear I-U curve in accordance with the ohmic current

conduction law[155], whereas conventional Ag/Pd, on the other hand, tends to form Schottky junctions with the sensor, which will indirectly affect the charge flow. In addition, it is also possible to directly cover the surface of LMNPs with semiconductors and form good contacts. WO_3 NPs on the surface of LMNPs can break the oxide layer and make direct contact with the liquid core, thus achieving ohmic current-like characteristics at the interface as well, and the sensitivity of the sensor is enhanced due to the better charge transfer efficiency at the WO_3/EGaIn interface[156], as shown in Figure 4A iv.

Furthermore, the good deformability of the LM as a conductive material for the sensor also allows for long-term resistance stability [Figure 4A v]. The normalized resistance of conductive materials filled with EGaIn microparticles can remain well stabilized during 2,500 stretches of 0% to 80% because of the 3D LM conductive network formed[157]. Another idea is to combine LM with some highly conductive nanomaterials. For example, when EGaIn microdroplets come into contact with nano-Ag flakes, the Ag flakes will cover the surface of the droplets and react to produce $AgIn_2$; a strong connection makes the material stretch so that it can cope with the deformation[158], thus achieving a stable resistance compatible with flexibility. Besides, it is also possible to use the breakage of the LMNPs and use the fluidity of LMs to repair the circuit to achieve the tensile stability of the material's resistance [Figure 4A v][159].

Chemical transformation
Sensor preparation
Regardless of the presence of oxygen in water, gallium can react with water to generate GaOOH microcrystals [Eq. (1)][160], such as LMNPs with surface-modified graphene quantum dots, which can promote the generation of GaOOH on the surface under light control, and can control the morphological transformation of LMNPs to realize the light-responsive LM "nano-transformer" [Figure 4B i]. In addition, the surface generation of GaOOH microcrystalline film will slightly reduce the passivation response of GaO generation. During the preparation and use of LM nanomaterials, the GaOOH on the LM surface should be continuously destroyed and generated to obtain LM droplets with smaller particle sizes and prevent particle fusion, while the storage of LMNPs can be optionally placed in organic solvents such as pure ethanol to avoid the formation of GaOOH.

$$Ga + 2H_2O \rightarrow GaOOH + 3H^+ \tag{1}$$

The GaOOH microcrystals generated from gallium will again react reversibly with water and ionize to form Ga^{3+} [Eq. (2)][161], a metal cation usually cross-linked as a ligand through its surface charge. For example, Xu *et al.* used gallium-based LMNPs to generate Ga^{3+} ions in the presence of H_2O and O_2 under the action of ultrasonic waves and formed a cross-linked PAA shell layer through the complexation of Ga^{3+} and -COO-, and this whole shell layer can be regarded as the "colloidal cross-linker" of the hydrogel [Figure 4B ii][161]. If the PAA network is disrupted, it will promote the production of free radicals and Ga^{3+}, and the free radicals and Ga^{3+} will cross-link again to achieve self-healing.

$$GaOOH + H_2O \rightarrow Ga^{3+} + 3OH^- \tag{2}$$

As discussed before, conductive pathways cannot be achieved for relatively independent individual LMNPs. Except for physical sintering, a chemical approach could also be applied to eliminate the oxide barrier. e.g., Li *et al.* performed rapid removal of surface oxides in HCl fume, brief chemical etching in HCl fume to

remove the oxide shell [Eq. (3)][162], resulting in a significant reduction in contact angle from 128° to 27°, and selective wetting of the unoxidized portion of the printed composite using Cu nanofillers in Galinstan microdroplets to achieve chemical sintering [Figure 4B iii].

$$Ga_2O_3 + 6HCl \rightarrow GaCl_3 + 3H_2O \qquad (3)$$

Chemical transformation is more than just a chemical reaction. The surface of LMNPs can also be further enhanced in terms of structural stability and multi-functionalization by modifying chemical groups. For example, the modification of thiols, such as 1-butanethiol and benzenethiol, can effectively prevent LMNPs from oxidation[163]. The modification of surfactants, such as Pluronic 127 (PF127), can enhance particle mechanical stability and prevent particle aggregation[164]. The modification of polyfunctional substances, such as polydopamine, can further modify other functional substances through electrostatic adsorption and chemical bonding[137]. Furthermore, modifying substances with conjugation potential, such as 4-mercaptopyridine, can enhance the electrical conductivity of LMNPs[163].

Sensing information detection and acquisition
Gallium oxide encapsulated on the surface of gallium NPs can change the resistance by gaining and losing electrons and act as a detection sensor for some typical redox chemicals. For example, based on the electron donor-acceptor mechanism, the reducing gas H_2 molecules lose electrons after the reaction, and the free electrons are captured by gallium oxide, leading to a gradual decrease in the resistance of n-type samples [Figure 4B iv]. Conversely, the oxidizing gas NO_2 molecules take away electrons from the gallium oxide, which leads to the gradual increase of the resistance of the n-type sample, thus achieving the accurate resistance change measurement [Eq. (4)][165]. Meanwhile, for different crystalline phases of gallium oxide, it was found that monoclinic phase gallium oxide can be produced in dimethyl sulfoxide (DMSO), while oblique crystalline phase gallium oxide is produced in water. As rhombic gallium oxide is not conducive to gas sensing, this makes gallium NPs in DMSO more sensitive than the gas in water[165].

$$2Ga + 3O^- \leftrightarrow Ga_2O_3 + 3e^- \qquad (4)$$

By ultrasonic nitriding at room temperature, GaN is formed on the surface of GaOOH crystals on the outside of LM microparticles [Eq. (5)][99], and the LM microparticles are rapidly transformed into LMNPs. At the same time, part of GaOOH and GaN are detached, and non-spherical particles consisting of orthorhombic α-GaOOH embedded in the domains of the hexagonal GaN structure are formed. As a 3.4 eV wide bandgap semiconductor material, gallium nitride has photoluminescence properties, which makes gallium NPs also have photoluminescence properties [Figure 4B v]. Since nitride has an adsorption effect on some organic substances, such as bovine serum albumin, the gallium NPs encapsulated with gallium nitride can detect its concentration by the burst effect to achieve accurate biosensing.

$$2Ga + N_2 \rightarrow 2GaN \qquad (5)$$

Other chemical bonds can be modified on the surface of gallium NPs, such as modifying sulfur bonds (-SH) to form gallium-sulfur covalent bonds [Eq. (6)][100] to connect gallium NPs with polymeric organic matter for specific biosensing. For example, based on the nature of gallium surface plasmon resonance, the 12-mer

specific DNA sequence of Helicobacter pylori can be selected as a component of R [5'-SH(CH2)-CAAAGGGCAGGA] and immobilized on gallium NPs to obtain GaNP with sulfurylated DNA capture probes, which gives the gallium plasma NPs sensing capabilities for label-free DNA and single nucleic acid polymorphism detection [Figure 4B vi].

$$RS - H + Ga_n \rightarrow RS^- Ga^+ Ga_n^0 + \frac{1}{2} H_2 \tag{6}$$
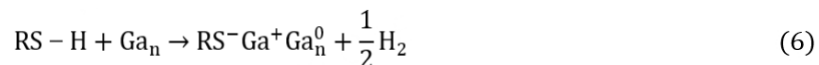
STRUCTURE OF THE NANO-LM SENSOR

Particulate (0D) nano-LM structures

Single LMNP sensing is no longer limited to mechanical deformation input and electrical signal output but is widely fused with optical, thermal, electrical, magnetic, ultrasonic, chemical signals and other sensing information for the application. Firstly, the catalytic range of LMNPs and their composite particles is wide and effective, which can not only reduce the catalytic activity of potassium ferricyanide and 4-nitrophenol[166] but also perform photocatalytic degradation of organic substances such as Congo red (CR)[167], and show high sensitivity to heavy metal ions including Hg^{2+} and Cd^{2+}[168,169]. For example, Zhang *et al*. constructed a heavy metal ion chemical catalytic sensor using nano-LMs. It was based on the advantage of the large surface area of NPs, the generation of the local electric field at the NP/LM/electrolyte triple-phase boundary enabling the sensing of heavy metal ions by measuring differential pulse voltammetry and they found that LM/MO was much more sensitive compared to LM droplets without any coating [Figure 5A i][168]. In fact, since gallium has no negative valence and does not undergo chemical reactions but only provides reaction sites for electrochemical reactions, the LM can effectively fuse heavy metal ions, which is not applicable to solid metal (SM). Therefore, a SM/MO framework cannot be directly compared with the LM/MO framework for heavy metal ion sensing performance, which reflects the unique advantage of LMs in the context of heavy metal ion sensors[168]. Secondly, unlike common noble metals, Ga has a dielectric constant function that extends from UV to the visible wavelength and continues to extend into the IR spectral region in the liquid form so that solid and liquid NPs or colloidal liquid Ga-based NPs have typical UV plasma properties. On the basis of UV plasma property characterization, Nucciarelli *et al*. designed the synthesis of Ga NP colloids for UV bio-optical sensors and experimentally verified the extremely strong UV response performance in tetrahydrofuran colloidal solution [Figure 5A ii][170]. In addition, Ga NPs are usually wrapped by Ga_2O_3, which provides protection for liquid Ga inside, and this MO film hardly affects the light propagation, so the plasma responsiveness remains unchanged[1]. In experiments of molecular beam epitaxy (MBE) deposition of Ga on sapphire substrates, unique solid-core liquid-shell NPs are formed due to the pressure of LM and oxide shells and at a certain range of higher temperatures without complete core melting. Roy *et al*. designed ionophore temperature response sensors based on the above properties [Figure 5A iii][1]. Finally, there are many other sensing techniques being explored for LMNPs, which illustrates the infusive research potential of nano-LM sensors.

LMNP-based one-dimensional (1D) circuit structures

The conductive path serves as one of the most fundamental and essential components in electronics to link functional elements and transmit electrical signals. Based on the transformability discussed above, LMNPs can be sintered to form simple conductive traces that serve as the very basic components in electronic devices. Boley *et al*. prepared EGaIn/ethanol/thiol dispersion and adopted spin-coating to fabricate a pre-activated surface on Kapton[171]. Subsequently, they displayed direct writing of high-resolution (down to about 1 μm in width) conductive trace initiated by mechanical force. This provided a facile approach to fabricating LM circuits in miniaturized devices. Based on this principle, Zhang *et al*. fabricated a flexible
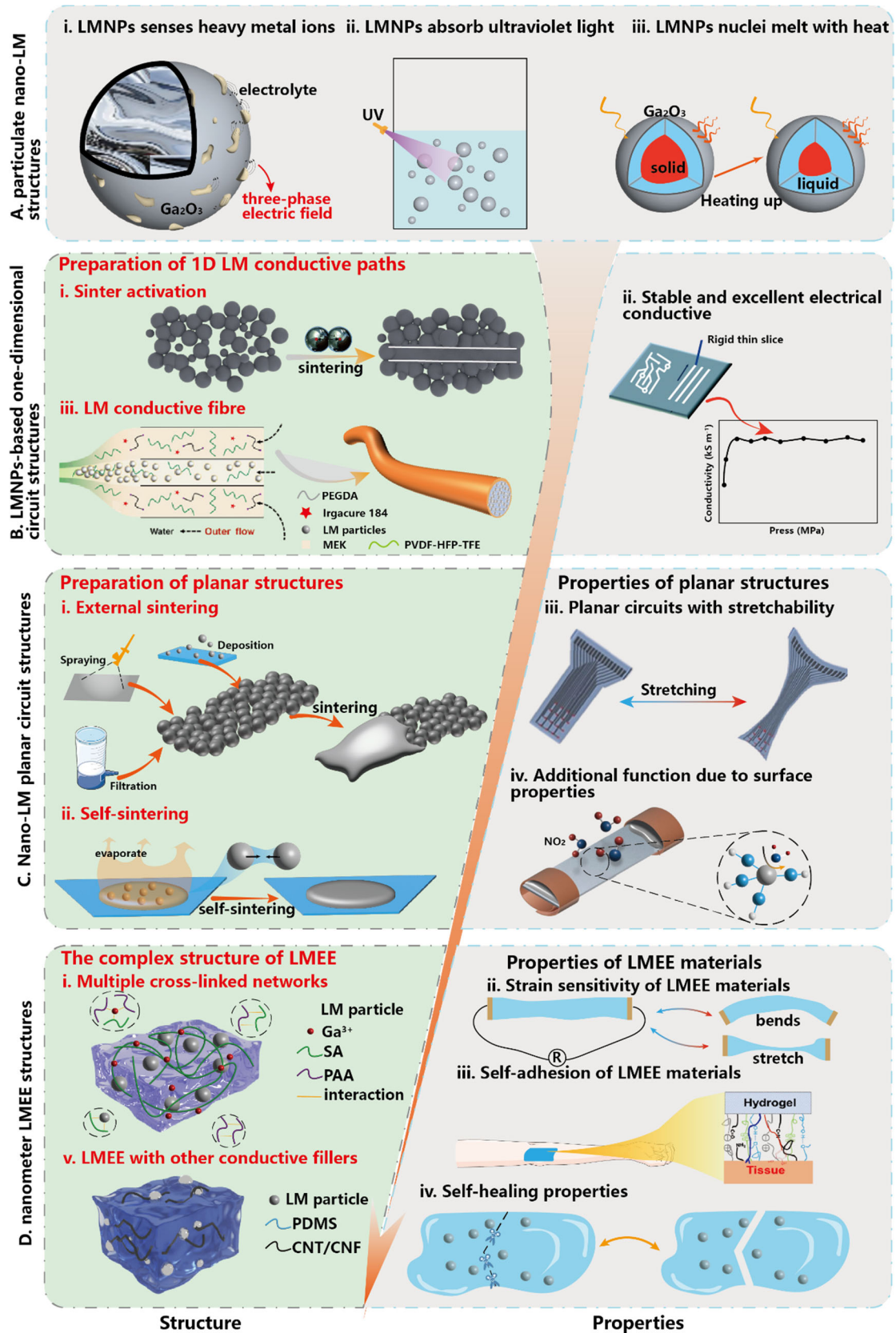
Figure 5. Different structures of nanofluid metal sensors and their applications or properties. (A) Particulate nano-LM structures: (i)

LMNPs are based on the induction of cadmium ions by a three-phase electric field; (ii) LMNPs absorb UV light; (iii) The solid-core liquid-shell structure of GaNPs senses temperature changes; (B) LMNPs-based one-dimensional circuit structures: (i) Preparation of conductive pathways from sintered nano-LMs; (ii) High conductivity of nano-LM circuits[174];(iii) Nano-LMs for the preparation of conductive fibres[178];(C) Nano-LM planar circuit structure: (i) Multiple ways of preparing plannar structures and sintering; (ii) Self-sintering of liquid metal to form planar structures; (iii) Stretchability of flat structures[184];(iv) Plane structures rich in other sensing properties[163];(D) Nanometer LM embedded elastomer structure: (i) Cross-linking network of LMEE; (ii) LMEE material with good strain sensitivity; (iii) Multiple interactions give LMEE materials self-adhesive properties[190];(iv) The strong self-healing capability of LMEE; (v) LMEE formed by multiple conductive fillers. CNF: Cellulose nanofiber; CNT: carbon nanotube; LMEE: LM embedded elastomer; LMNPs: LM nanoparticles; MEK: methyl ethyl ketone; PAA: poly(acrylic acid); PDMS: polydimethylsiloxane; PVDF-HFP-TFE: poly(vinylidene fluoride-hexafluoropropylene-tetrafluoroethylene); SA: sodium alginate; UV: ultraviolet.

Janus film through a spontaneous density deposition-induced self-assembly process [Figure 5B i][172]. The LMNPs deposited side could be facially activated into conductive paths via simple scratching. This work exhibited that it is possible to manufacture substrate-ink-integrated materials, which is optimistic for customized electronics. Similarly, Wu *et al.* prepared LM-LAPONITE ink to form a layered structure, and LMNPs could self-assemble under the effect of capillary force[173]. For healthcare applications, the biosafety and stability of materials are always of rigorous concern, so encapsulated LMNPs were developed[120,174,175]. Li *et al.* demonstrated that this practice was also suitable for LMNPs encapsulated in biocompatible hydrogel shells and realized conductive traces with the conductivity of $\sim 10^5$ S·m^{-1} on multiple substrates, including human skins [Figure 5B ii][174]. Laser sintering, as a kind of thermal sintering technique, further improves the conductivity of conductive paths up to 3×10^6 S·m^{-1}, which is comparable to the conductivity of bulk EGaIn[176,177]. These examples verified multiple accesses for LMNPs to coalesce into conductive traces on multiple substrates with high resolution, lower electrical resistivity, and customized patterns.

Although the displayed conductive paths in this section were actually areas instead of one-dimension "lines", the function they realized is simply the one-direction transmission of electrons and guarantees the most fundamental conduction in their works. Thus, we define such structures as the 1D form here; complex and more functionalized circuit structures are defined as the 2D form, which will be presented in the next section. Under this principle, besides activated conductive paths on substrates, LMNPs could also be fused in sheath-core fibers to work as cables. Zheng *et al.* applied the coaxial wet spinning method to fabricate a sheath-core fiber with PVDF-HFP-TFE [poly(vinylidene fluoride-hexafluoropropylene-tetrafluoroethylene)]/LM particles/MEK (methyl ethyl ketone) as core and PVDF-HFP-TFE/poly(ethylene glycol) diacrylate/Irgacure 184/MEK as a sheath, which was elastic and characterized as just slightly thicker than human hairs [Figure 5B iii][178]. Ning *et al.* reported a stretchable fiber composed of dimethyl formamide/LMNPs/PU as core and dimethyl formamide/PU as sheath[179]. The stable conductivity of such a structure was verified in a simple LED circuit under cycled stretching and relaxation state in their works.

The basic 1D form of LMNPs, which resulted in coalesced conductive structures, provided perspective for patterning intricate circuits on various substrates or combining LM-based fibers with fabrics[179] to constitute functional sensors.

Nano-LM planar (2D) circuit structure
In addition to conducting electrical signals, LM materials can also be a source of changes in electrical signals. Since the generation of electrical signals takes the form of the entire material plane and the information source is distributed throughout every point on the plane, we define this structure as a planar structure. To adjust the adhesion of LM on the surface, surfactants can be used to modify LMNPs[180]. The resulting LM electronic ink can adhere tightly to objects such as skin and balloons. Zhang *et al.* achieved rapid preparation of LM planar structures by preparing a thin layer of LMNPs by spraying[181]. Following a similar approach, Li *et al.* obtained a surface-functionalized nano-LM layer and "activated" the metal layer

by peeling off the upper and lower cover layers[182]. Apart from spraying, there are other methods to prepare planar structures, such as precipitation[183], filtration[155,180], *etc.* [Figure 5C i]. However, with the presence of oxide films, these methods still require sintering to create the conductive pathways[155,180,183,184]. However, most sintering methods have certain disadvantages, such as mechanical sintering, which still carries the risk of leakage, and laser sintering is difficult to scale up[184]. Therefore, it is ideal to avoid the sintering process and achieve self-sintering. Chiu *et al.* used conjugated thiol molecules attached to the Ga surface to form gallium-sulfur bonds to provide a pathway for electron flow between Ga particles, which inhibited the formation of oxide films and avoided the sintering process[163]. Park *et al.* used HCl and polyvinylpyrrolidone solution to remove the LM oxide film and stabilize the LM droplets, resulting in a thin (10-25 μm) and flat LM layer[185], as seen in Figure 5C ii.

The flexibility and electrical conductivity of LMs allow them to be used in many sensing devices. As bioelectrodes, LMs can be closely fitted to the human body and are able to work stably under conditions of intense movement and high stretching of the electrode material [Figure 5C iii][184]. The resistance between the LMNPs in the plane also changes due to deformation when subjected to stress[183], which can be used in sensors that monitor the movement of human muscles. In addition, surfactants also impart unique surface properties to the LM. Firstly, some surfactants can react with the targeted substance when combined with the LM. For example, 4-mercaptopyridine interacts non-covalently with NO_2 on the functionalized Ga metal surface[163], allowing the detection of NO_2 levels [Figure 5C iv]. Secondly, surfactants also contribute to the attachment of other substances to the surface of LM droplets, such as biological enzymes[186] or semiconductors[155,187], which allows LMs to form a planar reaction zone on the surface of the substrate with sweat secreted by the body, gases in the environment, *etc.* This is certainly an infusive feature for the functional enrichment of LM sensors. Furthermore, for self-powered sensors with multiple layers of friction, Yang *et al.* used a conventional sintering process to achieve material formation and prepared a composite film of LMNPs by ultrasonic dispersion and mechanical sintering, which was used as a friction layer with an encapsulation layer of PDMS[188]. The excellent flexibility and conductivity were achieved by combining the film as a friction layer with the encapsulation layer of PDMS, and the friction nanogenerator could achieve up to 268 V open-circuit voltage, 12.06 μA short-circuit current, and 103.59 nC transferred charge by replicating the PDMS friction layer into the microstructure using different master templates, which significantly enhanced the frictional charge density.

Nanometer LM embedded elastomer structure (3D)
In recent years, hydrogels have gained increasing interest in many biomedical applications because of their ability to convert stimuli during bioassay processes into electrical signals[189,190]. Other elastomers, such as rubbers, plastic polymers[151], *etc.*, are also being used more and more widely. To fabricate functional healthcare sensors, liquid-state precursors of these elastomers usually serve as base solvents to disperse conductive micro or nanoparticles. Under the effect of post-dispersion treatment, conductive fillers embedded elastomers are formed.

When LM micro/nanoparticles are embedded into composites with elastomer, the formed structure is always denoted as LM embedded elastomer (LMEE), where the oxide film on the surface of the droplet interacts with the polar groups (-OH, $-NH_2$, *etc.*[191]) of the organic matter, resulting in a stable and dispersed suspension distribution in the organic matter. Meanwhile, an extremely complex cross-linked network is formed in the LMEE [Figure 5D i]. For example, LM droplets mixed with acrylic acid (AA) form a double cross-linked network, both physically and chemically cross-linked [Figure 5D i][192]. It has also been shown that the addition of LM droplets accelerated the crosslinking process[191]. The good flexibility of both the matrix and the filler allows LMEE to have excellent tensile properties, even stretching to 2,200% of its length and still not breaking[192]. The mechanical properties and electrical conductivity of the composite can be

regulated by controlling the content of the NP. When the content of LMs is low, a complete conductive network cannot be formed in the elastomer. However, the distance between the LMNPs changes after applying stress, which causes a change in the resistance of the material. Based on this mechanism, LMEE can be used for strain-resistance type sensors [Figure 5D ii][154,193,194]. In addition, the good flexibility and electrical conductivity of the composite material also facilitate the detection of bioelectrical signals from the human body[192], and the abundance of polar groups allows LMEE to form rich hydrogen and coordination bonds with human skin and thus obtain self-adhesive properties [Figure 5D iii][190,192,195]. LMEE could also exhibit good self-healing properties by choosing appropriate substrates[196], e.g., LMNP/poly(3,4-ethylenedioxythiophene):sulfonated bacterial cellulose nanofiber (LMNP/PEDOT:BCNF) suspensions with AA can re-establish ion and electron transport channels within 0.16 s[197] [Figure 5D iv]. A new conductive sensor using LMNPs/MWCNTs/CNFs as multiphase hybrid fillers has also been prepared by incorporating a variety of highly conductive materials at the slight expense of the stretchable properties of the sensor[159], combining the high aspect ratio of CNTs with the fluid properties of LMs [Figure 5D v], which can reconstitute new connections for CNT/CNFs when subjected to large stresses within the oxide layer. In addition, the material exhibits excellent stress-strain-resistance sensitivity under low-strain conditions.

APPLICATION CATEGORIES
Motion monitoring
Movements of limbs are routinely adopted by hospital patients, especially for elderly individuals in recovery. The use of sensors for long-term monitoring of these behaviors can save significant medical resources and facilitate research data for patient recovery. The thin and sensitive nano-LM sensors can achieve monitoring and sensing without hindering human movement, which will greatly ameliorate the user experience. For instance, Zhang *et al.* produced an LM@CNC Janus film through a facile ultrasonication-deposition process and activated conductive paths on the LM side to realize a capacitive sensor[172]. The capacitive sensor was sensitive enough to detect the bending of the palm [Figures 6A and B], and the sensor showed good stability during 150 cycles of bending tests [Figure 6B]. The LM Janus membrane was made by using the sink of LM droplets, while LMs tend to be stably distributed in the suspension in more studies. For example, Feng *et al.* used a variety of interactions (chemical bonding, hydrogen bonding), the fabricated double cross-linked network cellulose-based LM hydrogel (LMCNF), as shown in Figure 6C, could be used to monitor the movement of human limbs[198], the relative resistance increased as the joint flexed. In addition, the sensor also has good sensitivity with a sensitivity factor of 2.92 over a strain range of 0% to 400% [Figure 6D]. Apart from direct monitoring of muscle movement, Liu *et al.* also reported a sensor capable of monitoring human breathing based on a polycaprolactone@LMNP thin film[199]. The film was placed onto an N95 mask along with a Bluetooth device to demonstrate the breath-monitoring function. The film was deformed by the airflow inhaled or exhaled by a volunteer, thus causing fluctuation in its resistance [Figure 6E]. To improve the biocompatibility of the sensors, using substances from human tissues as a matrix is a feasible solution. The researchers mixed gluten, which mainly consists of proteins, with EGaIn to make an EGaIn/gluten-based e-skin (E-GES)[200], which helped the matrix to form more β-sheets due to the fact that EGaIn induces new coordination and hydrogen bonds. The β-sheets are the most solid confirmation of gluten; thus, the increase of their content made the composite highly viscoelastic [Figure 6F]. Moreover, the E-GES could also be used as a strain gauge to monitor human movement, as bending during movement increases the resistance of the E-GES, and its superior stability allows the parameters to remain stable after more than 100 cycles. To further expand the application scenario of the sensor, Chen *et al.* realized a non-contact sensor at a longer distance (> 1 m) by simply adding ultrasonically treated EGaIn to a 3,4-ethylenedioxythiophene (EDOT) monomer solution containing EDOT[201], polystyrene sulfonate and ammonium persulphate to obtain a Ga-PP solution and immersing the textile in the solution to get a Ga-PP-based conductive textile (Ga-PP-CT), which uses the non-contact interaction between different charges to change the resistance of the sample [Figure 6G], thus allowing the monitoring of human movement such as jumping rope or playing tennis.
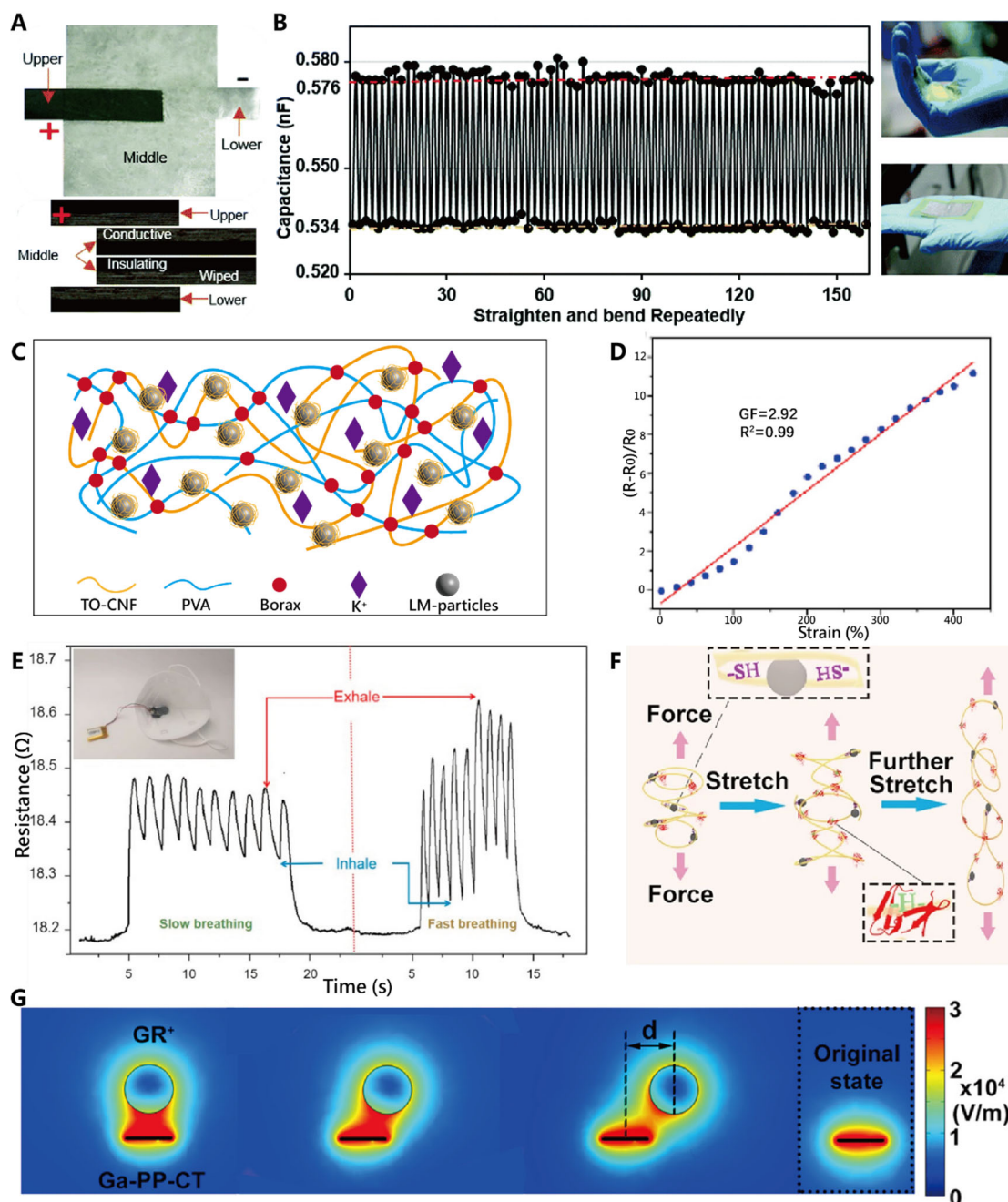
Figure 6. LM materials as sensors for motion monitoring. (A) Capacitive sensor prepared from Janus films[172]; (B) LM Janus membrane sensor for monitoring palm flexion movements[172]; (C) Structure and composition of LMCNF; (D) LMCNF sensors exhibit an excellent sensitivity[198]; (E) polycaprolactone@LMNPs for breath monitoring[199]; (F) Hydrogen bonding between βsheets and EGaIn-SH coordination bonds are favorable to improve the mechanical properties during stretching in E- GES[200]; (G) Sensor principle for non-contact sensors[201] (change in the electric field due to object movement). CNF: Cellulose nanofiber; E-GES: gluten-based e-skin; Ga-PP-CT: Ga-PP-based conductive; LM: liquid metal textile; PVA: poly(vinyl alcohol).

EMG signal detection

Unlike the monitoring of human muscle movement through strain, EMG sensors have been used to monitor the electrical signals of muscles using sensors that generate, conduct, and transmit potentials when the motor muscle is excited, which results in potential changes and triggered EMG signals. It could assist in determining the degree of muscle fatigue and other conditions, thus providing a credible evaluation of muscles. Lee *et al.* added LM droplets and polystyrene sulfonate to a solution containing acetic acid and formed stable polyelectrolyte-attached LM microgranular-particles (PaLMPs) conductive ink under ultrasonic treatment [Figure 7A][202]. The composite of the layer and substrate exhibited excellent mechanical and electrical properties and could continuously work for 10,000 cycles with a stable response. The sensor exhibited a high degree of fidelity when applied to monitoring EMG signals [Figure 7B]. In addition, based on their original study, they improved the conductivity of the sensor by using Pt-modified CNTs, namely Pt-decorated CNTs on gallium-based liquid-metal particles (CMP) with high electrical conductivity. Covered with LM droplets, the resulting LM ink was manifested with excellent wettability and high vapor pressure, which could conform and assemble the particles directly on the skin within 10 s[186]. The prepared myoelectric sensor was used to monitor the muscle electrical signals in the thighs of mice [Figure 7C]. After amplification of the signal by an external voltage, the signal of the CMP electrode was clear, whereas the normal LMNP electrode failed to detect the signal of muscle activation [Figure 7C], indicating that the sensor made of CMP had better electrical contact with the skin [Figure 7D]. The good biocompatibility of LMs makes *in vivo* biosensors possible. Based on EGaIn NPs, a three-layer structure bioelectrodes, as shown in Figure 7E, could detect EMG signals from 1 to 100,000 Hz in living organisms [Figure 7F], and this flexible electrode was simple to prepare and had a good performance, which was prospective for application[180].

Electrocardiographic (ECG) signal monitoring

Long-term monitoring of cardiac activity can help diagnose arrhythmias by identifying abnormal heartbeats. To this end, in addition to monitoring bioelectricity in biological muscles, nano-LMs have also been made into electrocardiographic (ECG) sensors. For example, Cao *et al.* first used thermoplastic PU-hexafluoroisopropanol to form fine and strong nanofibers, which were then combined with an isopropanol solution suspended with LMNPs by electrostatic spinning to form a nano-LM-based high-robust stretchable electrode (NHSE) with a thickness of 50 μm[203], where the LM conductive layer was several hundred nanometers in thickness. After 330,000 cycles from 0% to 100%, its resistance only increased by 5%, so NHSE shows excellent mechanical and electrical conductivity. When used as an electrode for monitoring human ECG signals, the contact impedance with the skin was comparable to that of commercial AgCl gel electrodes [Figure 8A]. In addition, it had higher sensitivity, as the signal measured by the NHSE remains almost constant during wrist movements. The NHSE also showed impressive waterproof capability, with little impact on sensing performance after being poured by water [Figure 8B]. In addition, the researchers also found that the ECG electrodes made of PaLMPs also had higher fidelity compared with commercial electrodes. They monitored in three places: left leg, left arm, and right arm, respectively, and the measured electrical signal data displayed more obvious peaks compared with those measured by commercial electrodes[202]. LM hydrogel complexes could also be used as ECG electrodes. The LM-SA (sodium alginate)-PAA hydrogel formed by mixing LMNP, SA, and AA had good self-adhesive properties and could be used as an ECG electrode material to detect human ECG signals in close proximity to the human epidermis [Figure 8C]. As shown in Figure 8D, the quality and stability of the measured ECG signals are better than those of commercial ECG electrodes[192].

Gas sensors

Gas concentration sensors

Not only can certain gas abnormalities be used in respiratory medicine as evidence of disease, but also
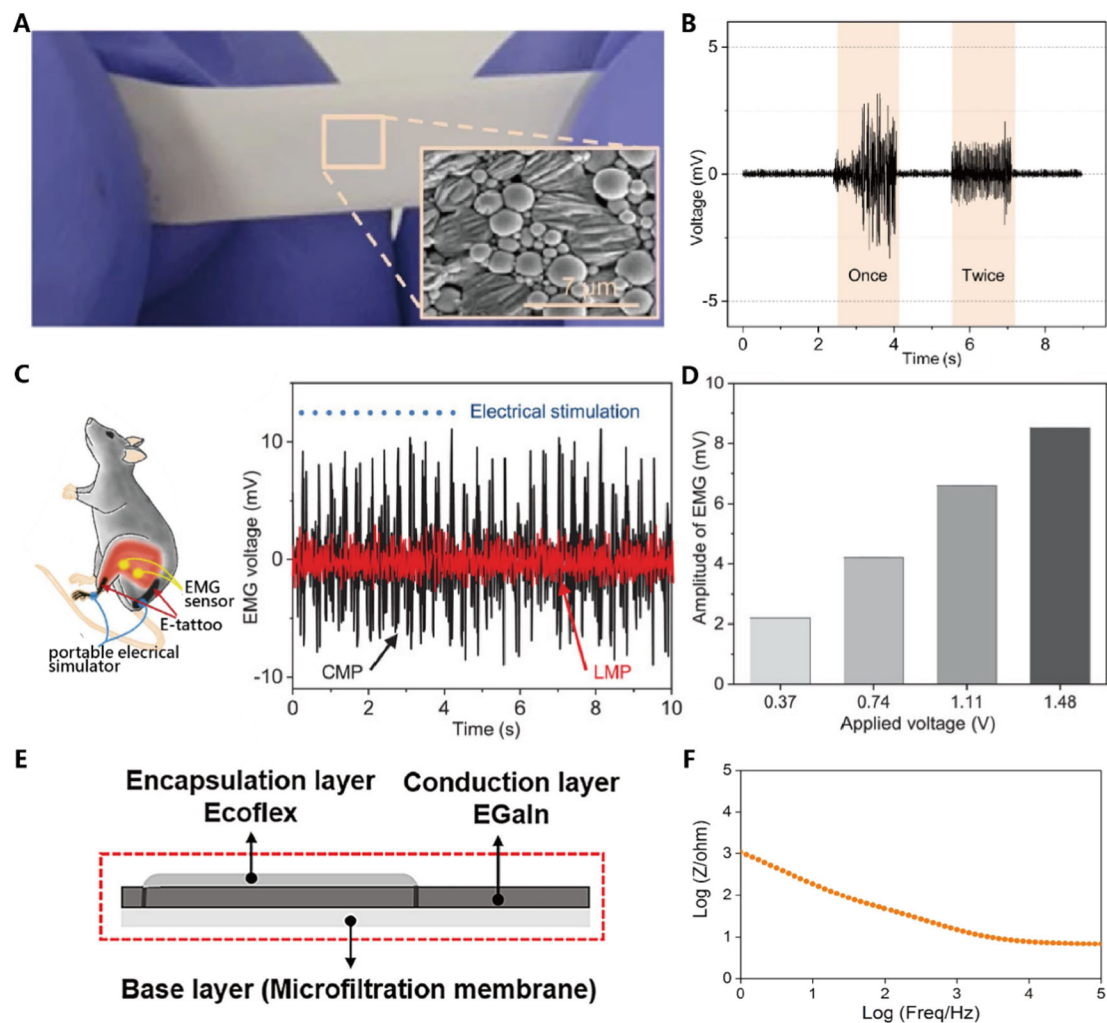
Figure 7. LM material for EMG information detection. (A) Photograph of a flexible EMG sensor manufactured on the basis of PaLMPs[202]; (B) EMG signal on the arm detected using the EMG sensor[202]; (C) Detection of EMG signals in the thighs of mice using sensor prepared from CMP vs. those prepared from common nano- LMs[186]; (D) The applied voltage is proportional to the EMG signal, indicating that the sensor has good contact with the skin[186]; (E) Schematic diagram of the three-layer structure of the implantable electrode[180]; (F) Impedance value of electrode related to frequency[180]. CMP: Liquid-metal particles; EGaln: eutectic gallium-indium alloy; EMG: electromyographic; LM: liquid metal; PaLMPs: polyelectrolyte-attached LM microgranular-particles.

certain irritant gases that can be very harmful to the human body are equally worthy of accurate monitoring. Based on the high electrical conductivity of LMs, it is possible to compound LM oxides[165] and other materials that inherently respond to certain gases[155,204]. Then, measuring the change in resistance could accurately reflect the changes in gas concentrations, such as NO, NO_2, H_2, HCl, *etc.* Specifically, Huang *et al.* prepared plastic electrodes by mechanically sintering nano-LM particles and added n-type semiconductor SnS_2 nanomaterials to design flexible breath sensors [Figure 9A i]. As SnS_2 sensed NO, electron transfer occurred, and SnS_2 changed from an electron-doped state to a hole-doped state, manifesting as a decrease in charge concentration and an increase in resistance, which further allows for highly sensitive asthma detection through NO changes [Figure 9A ii][155,205]. In addition, considering that exhaled H_2O may be ionized as H_2O^+, the electrons of water vapor will be transferred to SnS_2. Resistance change could also be used to accurately determine exhalation, inhalation, and static state [Figure 9A iii][155]. For other substance interference, the response was stable at 70% or less for NO of 50 ppb under the interference of H_2, CH_4, NH_3 of 500 ppb or VOC of 100 ppm, where the temperature change (4.5 to 34.3 °C)
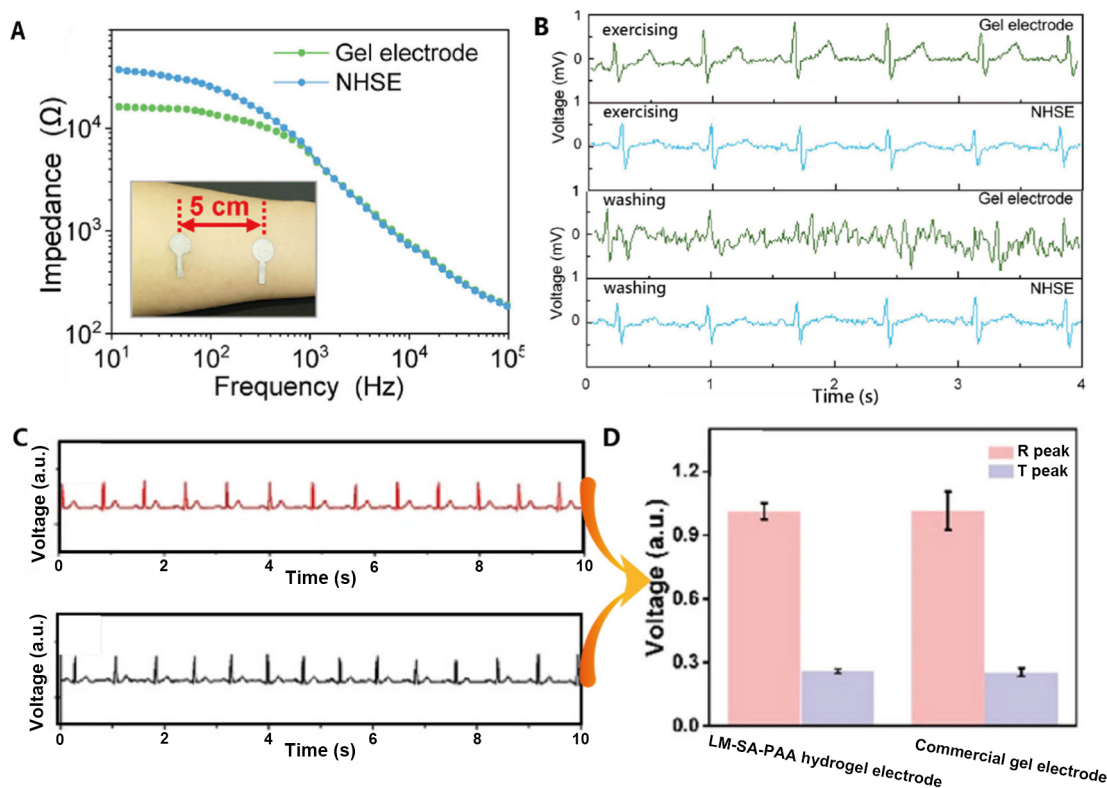
Figure 8. Application of LM materials in ECG sensors. (A) Contact impedance of NHSE electrodes and commercial gel electrodes to the skin[203]; (B) Comparison of ECG signals measured by NHSE electrodes and commercial gel electrodes during exercise and washout, respectively[203]; (C) ECG signals measured using LM-SA-PAA hydrogel electrodes (upper) and commercial electrodes (lower)[192]; (D) T/R peak ratios and baseline deviations between T and P waves for commercial gel electrodes and LM-SA-PAA hydrogel electrodes[192]. ECG: Electrocardiographic; LM: liquid metal; NHSE: nano-LM-based high-robust stretchable electrode; PAA: poly(acrylic acid); SA: sodium alginate.

and CO effect could be approximately neglected (< 2%). For the impact of water vapor, the NO sensing sensitivity decreased by 10% at 90% humidity, but the reaction rate increased by ~19%, which was probably due to a more abundant ionized form of SnS_2, resulting in additional electrons provided for NO. For the effect of CO_2, since CO_2 is also an oxidizing gas, it may make the reversal concentration of NO lower than 58 ppb, which is close to the upper limit of 51.1 ppb of NO concentration in normal human breath. Therefore, even though NO sensing was not found to be affected by H_2O and CO_2 during the existing respiratory monitoring, the effect of CO_2 should still be additionally considered in practical use[155]. Similarly, Zhang *et al*. designed a polyaniline (PANI)-EGaIn nanocomposite chemical sensor for HCl vapor based on the inherent response of PANI to HCl vapor [Figure 9B][204]. This composite had stronger stability and response compared with the conventional PANI film due to the enhanced conductivity caused by the corrosion of the dense oxide on the LM surface by HCl.

Gas pressure sensor
Air pressure directly affects the supply of oxygen to the human body, so it is essential to determine the change in gas pressure[206]. Based on the expansion and compression of the hydrogel to change the conductive pathway resistance, Zhang *et al*. creatively proposed a flexible vacuum sensor by preparing a PAA-LM/reduced graphene oxide (PAA-LM/rGO) hydrogel containing a microporous structure formed by hydrogen gas generated by the reaction of Ga with hydrogen ions, and this flexible and porous structure provides the feasibility for vacuum level detection[189]. Specifically, as the atmospheric pressure decreased,
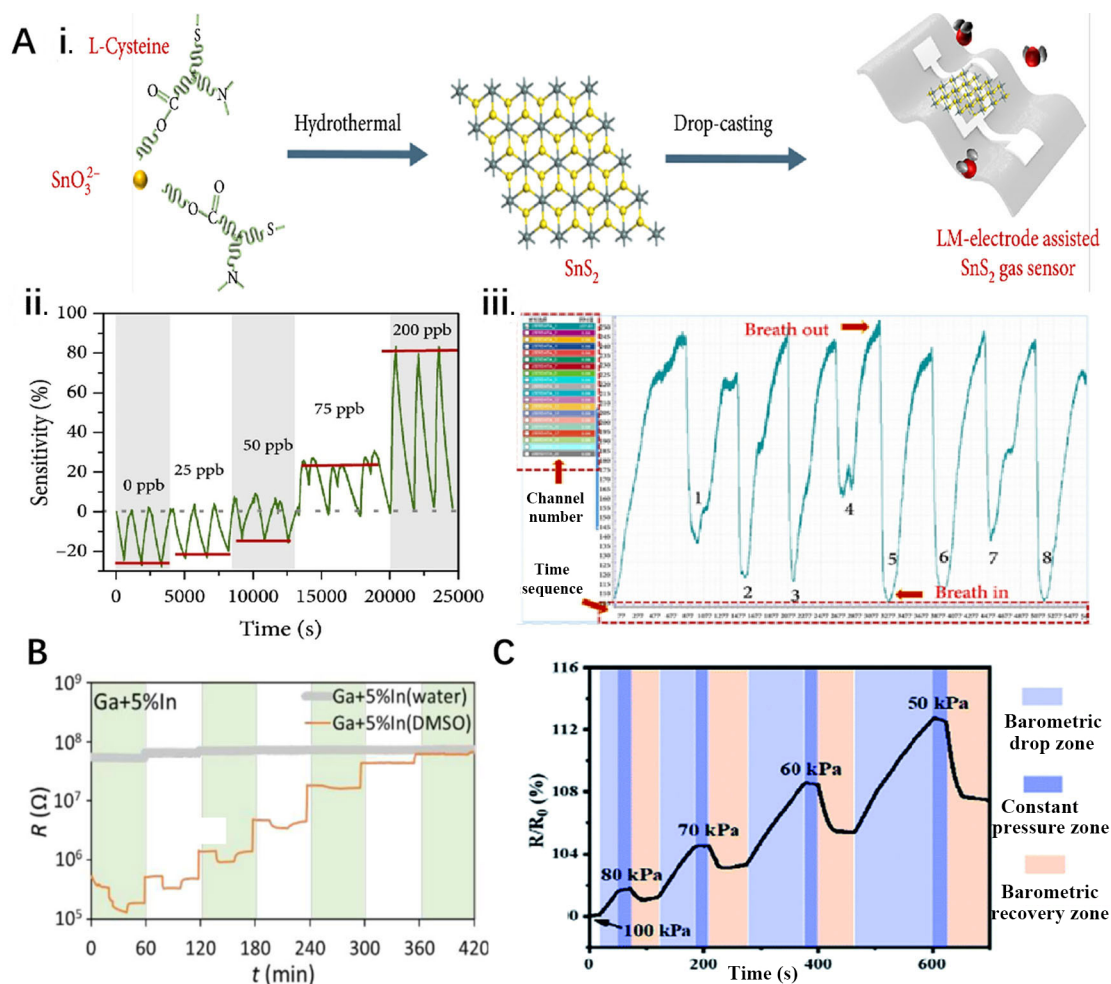
Figure 9. Application of LMNPs in gas sensors. (A) LM-SnS$_2$ gas sensor[155]. (i) Schematic diagram of preparation processes; (ii) Schematic diagram of NO sensing detection at different concentrations; (iii) Schematic diagram of real-time respiration monitoring (monitoring of H$_2$O); (B) Schematic diagram of HCl sensing detection[204]. (C) Schematic diagram of gas pressure sensing detection[189]. DMSO: Dimethyl sulfoxide; LM liquid metal; LMNPs: LM nanoparticles.

the void volume increased, leading to an increase in the overall volume of the hydrogel, which further allowed the measurement of increased resistance to indicate the vacuum level, which provides a preventable solution for diseases related to the effects of air pressure such as pulmonary edema, stroke, and heart disease. In the actual test, during the change from standard atmospheric pressure (100 KPa) to negative air pressure (50 KPa), the resistance in the hydrogel sensor rose from 0.5% to 6% [Figure 9C], and conversely, increasing air pressure resistance gradually recovered. However, due to water loss and irreversible deformation, the resistance value might be slightly higher than the initial resistance.

Temperature sensor

Expansion-type temperature sensor
Wang *et al.* prepared a composite hydrogel of cross-linked chitosan quaternary ammonium salts and EGaIn particles, which has a dual response to stress and temperature [Figure 10A i][207]. The hydrogels exhibit declined resistance for temperature sensing in response to increasing temperature. This was due to the fact that the temperature affected the mobility of LMs, resulting in conductive paths that are affected by
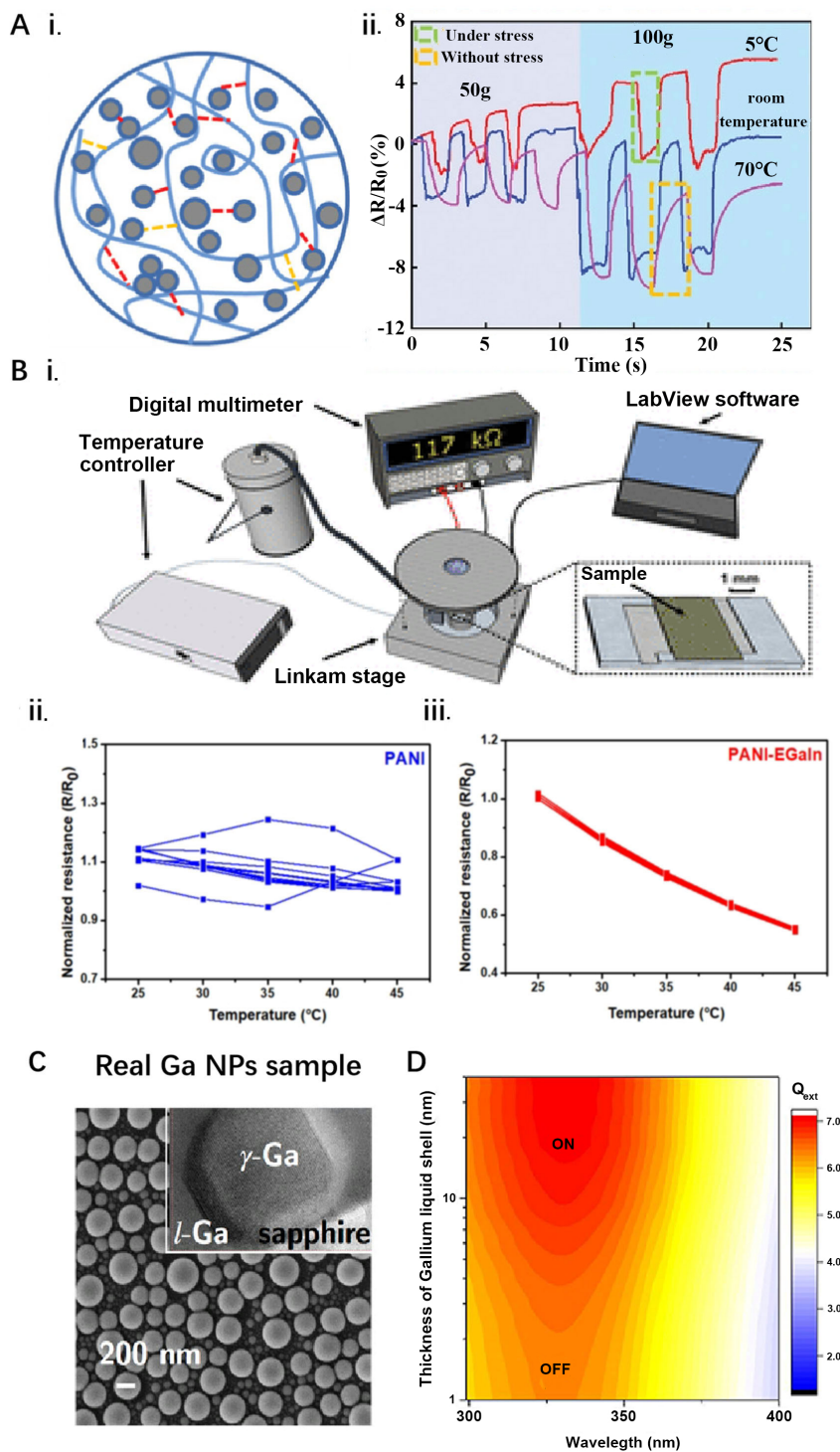
Figure 10. Application of LMNPs in temperature sensors. (A) (i) Schematic diagram of LM composite hydrogel[207];(ii) Schematic diagram of resistance vs. temperature for hydrogels[207]; (B) (i) Physical diagram of temperature sensor devices[208]; Schematic diagram of resistance vs. temperature for normalized pure PANI (ii) and PANI with composite EGaIn (iii)[204]; (C) SEM and TEM (inset) of actual samples of Ga NPs deposited on sapphire substrates[209]; (D) Plot of extinction efficiency of different liquid metal layer thicknesses on sapphire[1]. EGaIn: Eutectic gallium-indium alloy; LM: liquid metal; NPs: nanoparticles; PANI: polyaniline.

temperature. This property was manifested over a wide range of temperatures, even in the low-temperature

temperature region. It has been verified that the hydrogel resistance decreased as a function of temperature from 25 to 70 °C. However, the stress could also affect the conductive path, so the stress variable should be controlled the same to detect the difference in temperature. For example, the hydrogel showed a logarithmic increase in resistance from fast to slow when exposed to the reagent at 5 °C, the opposite trend when exposed to the reagent at 70 °C, and no significant electrical signal at 25 °C [Figure 10A ii][207]. Kim *et al.* and Zhang *et al.* designed temperature sensors with similar principles as above [Figure 10B i] but supplemented by measuring the resistance change of pure isopropylacrylamide[208] and pure PANI[204] at different temperatures, respectively [Figure 10B ii and iii], illustrating that the resistance of hydrogel without LMs was not affected by temperature, further indicating that the material that causes the resistance change due to temperature change is LM particles instead of the hydrogel.

Plasma temperature sensors
Roy *et al.*, based on the phase change plasmonic nature of Ga NPs, proposed plasma temperature sensors and verified their feasibility by simulation and experiments[1]. Firstly, the Ga NPs used here are in a core-shell structure (internal solid - intermediate liquid - external MO film), as shown in Figure 10C[209]. This particular core γ-Ga was prepared by MBE deposition on a sapphire substrate. In terms of the nucleation mechanism, the Ga NPs have a contact angle of about 130° on the sapphire, and this high curvature leads to high Laplace pressure, which, in turn, propels the generation of γ-Ga[209,210]. Although the solid cores gradually melt with increasing temperature, some of the solid cores are retained due to the pressure of the intervening liquid and the outer MO. Therefore, if the change of the oxide layer was not considered, the thickness of the intermediate LM layer represented the change of temperature if the radius of the control particles was certain. In the temperature sensing test, the particles were placed on top of a sapphire substrate, which represented experimental conditions with room temperature conditions, suitable surface energy for solid nucleation, and highly transparent and non-fluorescent in the experimental range. The extinction efficiency diagram of Ga core-shell structures on sapphire with different thicknesses of the liquid shell shows that the extinction cross section at the resonance gradually decreases as the size of the liquid shell layer decreases, and the deep red region at the dipole resonance corresponding to the thicker liquid shell disappeared when the size of the liquid shell layer decreased to a certain degree, which indicated that the impact field started to interact with the solid core [Figure 10D][1]. Also, the ON in the figure indicates high extinction and OFF indicates low extinction. This contrast also reflects the feasibility of temperature plasma switching.

Other applications
In addition to the above features, Zhang *et al.* fabricated LM/MO spherical structures, which were found to be highly sensitive to low concentrations of heavy metal ions (Pt^{2+}), and then the local electric field at the boundary of the NP/LM/electrolyte triple phase formed by combining with other NPs (e.g., WO_3) would further improve the sensitivity of the sensor[168]. Ambient sound also affects human health by reducing human sleep and other effects, and researchers have found that their resistance changes significantly when affected by acoustically induced air vibrations through a synthesized nano-LM flexible sensor, enabling the detection of ambient sound quality[199]. Researchers have also prepared a kirigami-structured LM paper (KLP), which gives the otherwise unstretchable paper a stretchable structure through a paper-cutting process [Figure 11A], and KLP was used as an electroencephalographic (EEG) sensor to monitor brain activity accurately [Figure 11B and C][211]. LMs could also be used to monitor the composition of sweat [Figure 11D]. Using the electrochemical properties of LMs and CNTs, for instance, CNTs can provide sites for enzyme immobilization; it is possible to convert the content of certain components of sweat into electrical signals[186] [Figure 11D].
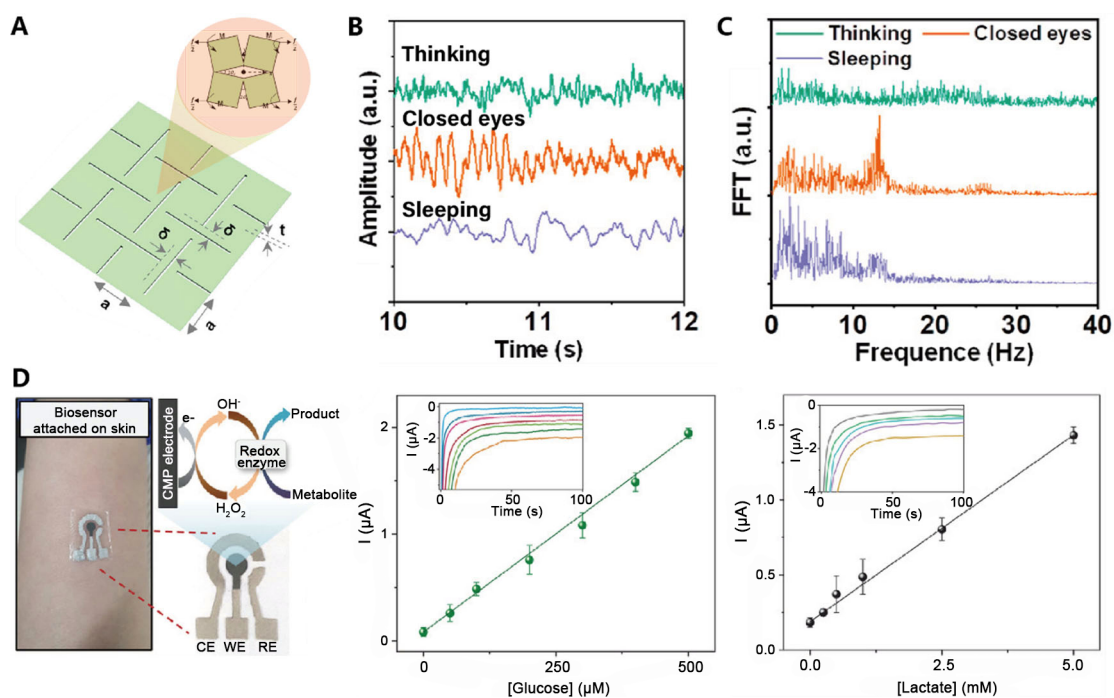
Figure 11. Other applications for LM material sensors. (A) KLP structure and the principle of stretchability[211]; (B) Three EEG signals for different mental states[211]; (C) Frequency distribution of EEG signals after FFT processing[211]; (D) Schematic diagram of the sweat sensor and test results on the concentration of selected biomarkers[186]. EEG: Electroencephalographic; KLP: kirigami-structured LM paper; LM: liquid metal.

SUMMARY AND OUTLOOK

With their excellent tensile properties, electrical conductivity, and other properties, LMs are widely studied in sensors, and LM nanotransformers not only inherit the high electrical conductivity and flexibility of macroscopic LMs but also have the properties of easy dispersion, flexible deformation, and multiple modification and fusibility, which bring a series of development of connected intelligent health care sensors. In this paper, the latest research of nano-LM sensors in the field of human life and health is presented, and their research in the direction of human motion monitoring, electrophysiological signal monitoring (EEG, ECG, EMG), temperature, gas, and medical imaging gradually show the great potential and advantages brought by the superior physical and chemical properties of LMs. These sensors will greatly help monitor and diagnose human life and health. The main substances of LMNPs, such as gallium (206.92 $/kg) and indium (284.2 $/kg), are relatively expensive compared to conventional materials, such as copper (9.23 $/kg), aluminum (2.72 $/kg), and CNTs (0.12 $/kg) (These data were recorded on 2023.9.29 at https://jiage. cngold.org/), but the dosage of LMNPs in sensors is relatively small, e.g., the dosage of LM in one LMNPs epidermal flexible sensor is is only about 3 g, so the actual cost is not high. At the same time, LMNPs have high flexibility compared to traditional metals, high electrical conductivity compared to CNTs, and unique liquid-liquid interface, liquid-solid interface, phase transition properties, optical properties, and many other characteristics that make LMNP sensors have irreplaceable value. In addition, gallium-based LMs are more versatile and have a larger liquid temperature range, which can cope with the ambient temperatures of most human activities. It is also beneficial for the liquid metal to remain liquid due to the constant heat dissipation by the human body and the fact that the encapsulation layer prevents a certain degree of convective heat transfer from the outside world. However, solidification of the LM is still unavoidable at lower temperatures and can be prevented by external fields such as electric fields using Joule heating.

From the perspective of sensor improvement, the accuracy of the data acquired by sensors should be further improved, for example, by using implantable sensors for key areas to further reduce the distance to the measurement object and considering the sensor wrapped around blood vessels for direct measurement to minimize the loss of information through the skin and muscles to obtain more accurate physical details. At the same time, the comprehensiveness of sensor measurement information is also worth improving. For example, by manufacturing spatially anisotropic material, pressure sensors can accurately calculate the magnitude and direction of pressure. Moreover, the source of sensor information should be further enriched, for example, by exploiting the properties of nanoscale Ga_2O_3 electrolytic iridescence on LM surfaces[95], thus responding to and sensing a certain stimulus. In addition, for practical application and portable convenience, making the sensors extremely miniaturized and flexible is a hotspot. For instance, using magnetic/electric field modulation of the LM can make the extremely small sensors swim in the blood vessels rather than be fixed in a specific position. Finally, regarding the complexity and integration of sensor functions, the current nano-LM sensors are limited to the nature of the LM itself or a single sensor to function independently, so whether it is the use of LMs and their organic/inorganic composite materials of complex functions of the combination or the preparation of multi-functional or joint use of sensors is the direction that requires in-depth consideration by researchers.

From the perspective of sensor innovation, on the one hand, although most of the properties of LMNPs are well used in the field of sensors, some of them are poorly understood and not yet explored in depth for applications, such as GaOOH shell-LM core NPs subjected to photoinduced deformation have potential as optical sensors[160], and LMNPs with surface plasmon resonance features are also expected to create surface plasmon resonant biosensors[1], LMNPs based on size effects and phase transition capabilities have unique advantages for preparing sensors across the solid-liquid temperature band[212], UV plasma properties of LM NPs also deserve to be studied in depth in the field of imaging[213]. On the other hand, accurate and in-depth data processing reflects digital and intelligent innovation, which is an inevitable trend in sensor development, so it is necessary to analyze the output of some sensing signals to obtain functional links, such as the correspondence between chemotherapy drug concentration and photothermal treatment temperature[120], the correspondence between current and motion state of friction nanogenerators[214], the correspondence between phase transition process of LMNPs and solvent temperature, and so on. The exploration of these functional relationships will greatly enhance the data analysis capability and application value of LM nanotransformer-based biosensors and play a very important role in the further development of nano-LM sensors.

DECLARATIONS

Authors' contributions
Proposed original conceptualization: Rao W
Investigated the related work: Bai Y, Zhang J
Prepared the figures and wrote the article: Bai Y, Zhang J, Lu C
Revised and corrected article: Bai Y, Zhang J, Lu C
Supervised the manuscript: Lu C, Rao W

Availability of data and materials
Not applicable.

Conflicts of interest

All authors declared that there are no conflicts of interest.

Ethical approval and consent to participate

Not applicable.

Consent for publication

Not applicable.

Copyright

© The Author(s) 2023.

REFERENCES

1. Roy P, Bolshakov AD. Temperature-controlled switching of plasmonic response in gallium core-shell nanoparticles. *J Phys D Appl Phys* 2020;53:465303. DOI

2. Quesada-González D, Merkoçi A. Nanomaterial-based devices for point-of-care diagnostic applications. *Chem Soc Rev* 2018;47:4697-709. DOI PubMed

3. Gu Y, Zhang T, Chen H, et al. Mini review on flexible and wearable electronics for monitoring human health information. *Nanoscale Res Lett* 2019;14:263. DOI PubMed PMC

4. Ullah H, Wahab MA, Will G, et al. Recent advances in stretchable and wearable capacitive electrophysiological sensors for long-term health monitoring. *Biosensors* 2022;12:630. DOI PubMed PMC

5. Zheng A, Qin Y, Zhang X, Xia Q, Xu X, Bai C. Tentacled snakes-inspired flexible pressure sensor for pain sensation monitoring. *Smart Mater Struct* 2022;31:045004. DOI

6. Song D, Li X, Li XP, Jia X, Min P, Yu ZZ. Hollow-structured MXene-PDMS composites as flexible, wearable and highly bendable sensors with wide working range. *J Colloid Interface Sci* 2019;555:751-8. DOI

7. Sun P, Wu D, Liu C. High-sensitivity tactile sensor based on Ti$_2$C-PDMS sponge for wireless human-computer interaction. *Nanotechnology* 2021;32:295506. DOI PubMed

8. Li S, Gu Y, Wu G, et al. A flexible piezoresistive sensor with highly elastic weave pattern for motion detection. *Smart Mater Struct* 2019;28:035020. DOI

9. Li KH, Cheung YF, Choi HW. Tunable GaN photonic crystal and microdisk on PDMS flexible films. *ACS Appl Electron Mater* 2019;1:1112-9. DOI

10. Ruiz JAR, Sanjuán AM, Vallejos S, García FC, García JM. Smart polymers in micro and nano sensory devices. *Chemosensors* 2018;6:12. DOI

11. Sang S, Jing Z, Cheng Y, Ji C, Zhang Q, Dong X. Graphene and MXene-based sponge pressure sensor array for rectal model pressure detection. *Macro Mater Eng* 2021;306:2100251. DOI

12. Xu B, Ye F, Chen R, Luo X, Chang G, Li R. A wide sensing range and high sensitivity flexible strain sensor based on carbon nanotubes and MXene. *Ceram Int* 2022;48:10220-6. DOI

13. Qin Y, Peng Q, Ding Y, et al. Lightweight, superelastic, and mechanically flexible graphene/polyimide nanocomposite foam for strain sensor application. *ACS Nano* 2015;9:8933-41. DOI

14. Pu L, Liu Y, Li L, et al. Polyimide nanofiber-reinforced Ti$_3$C$_2$T$_x$ aerogel with "lamella-pillar" microporosity for high-performance piezoresistive strain sensing and electromagnetic wave absorption. *ACS Appl Mater Interfaces* 2021;13:47134-46. DOI

15. Liu H, Chen X, Zheng Y, et al. Lightweight, superelastic, and hydrophobic polyimide nanofiber/MXene composite aerogel for wearable piezoresistive sensor and oil/water separation applications. *Adv Funct Mater* 2021;31:2008006. DOI

16. Dai Y, Wu X, Liu Z, Zhang HB, Yu ZZ. Highly sensitive, robust and anisotropic MXene aerogels for efficient broadband microwave absorption. *Compos B Eng* 2020;200:108263. DOI

17. Luo S, Hoang PT, Liu T. Direct laser writing for creating porous graphitic structures and their use for flexible and highly sensitive sensor and sensor arrays. *Carbon* 2016;96:522-31. DOI

18. Zhao Y, Song JG, Ryu GH, et al. Low-temperature synthesis of 2D MoS$_2$ on a plastic substrate for a flexible gas sensor. *Nanoscale* 2018;10:9338-45. DOI

19. Kenry, Yeo JC, Lim CT. Emerging flexible and wearable physical sensing platforms for healthcare and biomedical applications. *Microsyst Nanoeng* 2016;2:16043. DOI PubMed PMC

20. Gao Y, Fang X, Tan J, Lu T, Pan L, Xuan F. Highly sensitive strain sensors based on fragmentized carbon nanotube/ polydimethylsiloxane composites. *Nanotechnology* 2018;29:235501. DOI

21. Zhao Y, Ren M, Shang Y, et al. Ultra-sensitive and durable strain sensor with sandwich structure and excellent anti-interference ability for wearable electronic skins. *Compos Sci Technol* 2020;200:108448. DOI

22. Pu JH, Zhao X, Zha XJ, et al. A strain localization directed crack control strategy for designing MXene-based customizable sensitivity and sensing range strain sensors for full-range human motion monitoring. *Nano Energy* 2020;74:104814. DOI

23.   Wang H, Zhou R, Li D, et al. High-performance foam-shaped strain sensor based on carbon nanotubes and $Ti_3C_2T_x$ MXene for the monitoring of human activities. *ACS Nano* 2021;15:9690-700. DOI

24.   Li X, Yang J, Yuan W, et al. Microstructured MXene/polyurethane fibrous membrane for highly sensitive strain sensing with ultra-wide and tunable sensing range. *Compos Commun* 2021;23:100586. DOI

25.   Wei Q, Chen G, Pan H, et al. MXene-sponge based high-performance piezoresistive sensor for wearable biomonitoring and real-time tactile sensing (Small Methods 2/2022). *Small Methods* 2022;6:2270012. DOI

26.   Yue Y, Liu N, Liu W, et al. 3D hybrid porous Mxene-sponge network and its application in piezoresistive sensor. *Nano Energy* 2018;50:79-87. DOI

27.   Zhao L, Wang L, Zheng Y, et al. Highly-stable polymer-crosslinked 2D MXene-based flexible biocompatible electronic skins for in vivo biomonitoring. *Nano Energy* 2021;84:105921. DOI

28.   Qin R, Li X, Hu M, Shan G, Seeram R, Yin M. Preparation of high-performance MXene/PVA-based flexible pressure sensors with adjustable sensitivity and sensing range. *Sens Actuator A Phys* 2022;338:113458. DOI

29.   Zhang R, Deng H, Valenca R, et al. Carbon nanotube polymer coatings for textile yarns with good strain sensing capability. *Sens Actuator A Phys* 2012;179:83-91. DOI

30.   Huang J, Li D, Zhao M, et al. Highly sensitive and stretchable CNT-bridged AgNP strain sensor based on TPU electrospun membrane for human motion detection. *Adv Elect Mater* 2019;5:1900241. DOI

31.   Sun J, Zhou W, Yang H, et al. Highly transparent and flexible circuits through patterning silver nanowires into microfluidic channels. *Chem Commun* 2018;54:4923-6. DOI

32.   Hao Y, Gao J, Xu Z, Zhang N, Luo J, Liu X. Preparation of silver nanoparticles with hyperbranched polymers as a stabilizer for inkjet printing of flexible circuits. *New J Chem* 2019;43:2797-803. DOI

33.   Wei Y, Chen S, Dong X, Lin Y, Liu L. Flexible piezoresistive sensors based on "dynamic bridging effect" of silver nanowires toward graphene. *Carbon* 2017;113:395-403. DOI

34.   Choi Y, Kang J, Secor EB, et al. Capacitively coupled hybrid ion gel and carbon nanotube thin-film transistors for low voltage flexible logic circuits. *Adv Funct Mater* 2018;28:1802610. DOI

35.   Xu X, Chen Y, He P, et al. Wearable $CNT/Ti_3C_2T_x$ MXene/PDMS composite strain sensor with enhanced stability for real-time human healthcare monitoring. *Nano Res* 2021;14:2875-83. DOI

36.   Xu X, Luo M, He P, Guo X, Yang J. Screen printed graphene electrodes on textile for wearable electrocardiogram monitoring. *Appl Phys A* 2019;125:714. DOI

37.   Hosseinzadeh A, Bidmeshkipour S, Abdi Y, Arzi E, Mohajerzadeh S. Graphene based strain sensors: a comparative study on graphene and its derivatives. *Appl Surf Sci* 2018;448:71-7. DOI

38.   Zhang R, Pan P, Dai Q, et al. Sensitive and wearable carbon nanotubes/carbon black strain sensors with wide linear ranges for human motion monitoring. *J Mater Sci Mater Electron* 2018;29:5589-96. DOI

39.   Wang H, Yao Y, He Z, et al. A highly stretchable liquid metal polymer as reversible transitional insulator and conductor. *Adv Mater* 2019;31:1901337. DOI

40.   Chang H, Guo R, Sun Z, et al. Direct writing and repairable paper flexible electronics using nickel-liquid metal ink. *Adv Mater Interfaces* 2018;5:1800571. DOI

41.   Wang Y, Zhang P, Tan S, et al. Experimental and numerical analysis on a compact liquid metal blade heat dissipator with twin stage electromagnetic pumps. *Int Commun Heat Mass Transf* 2019;104:15-22. DOI

42.   Chen S, Deng Z, Liu J. High performance liquid metal thermal interface materials. *Nanotechnology* 2021;32:092001. DOI PubMed

43.   Wang X, Lu C, Rao W. Liquid metal-based thermal interface materials with a high thermal conductivity for electronic cooling and bioheat-transfer applications. *Appl Therm Eng* 2021;192:116937. DOI

44.   Deng Y, Jiang Y, Liu J. Liquid metal technology in solar power generation - Basics and applications. *Sol Energy Mater Sol Cells* 2021;222:110925. DOI

45.   Chen S, Wang L, Zhang Q, Liu J. Liquid metal fractals induced by synergistic oxidation. *Sci Bull* 2018;63:1513-20. DOI

46.   Li DD, Liu TY, Ye J, Sheng L, Liu J. Liquid metal-enabled soft logic devices. *Adv Intell Syst* 2021;3:2000246. DOI

47.   Liu TY, Li DD, Ye J, Li Q, Sheng L, Liu J. An integrated soft jumping robotic module based on liquid metals. *Adv Eng Mater* 2021;23:2100515. DOI

48.   Shaini FJ, Shelton RM, Marquis PM, Shortall AC. In vitro evaluation of the effect of freshly mixed amalgam and gallium-based alloy on the viability of primary periosteal and osteoblast cell cultures. *Biomaterials* 2000;21:113-9. DOI PubMed

49.   Wang D, Lu C, Wang X, Rao W. In-situ synthesized liquid metal microgels. In: 2021 IEEE 16th International Conference on Nano/Micro Engineered and Molecular Systems (NEMS); 2021 Apr 25-29; Xiamen, China. IEEE; 2021. p. 469-73. DOI

50.   Hou Y, Zhang P, Wang D, Liu J, Rao W. Liquid metal hybrid platform-mediated ice-fire dual noninvasive conformable melanoma therapy. *ACS Appl Mater Interfaces* 2020;12:27984-93. DOI PubMed

51.   Kalantar-Zadeh K, Tang J, Daeneke T, et al. Emergence of liquid metals in nanotechnology. *ACS Nano* 2019;13:7388-95. DOI

52.   Dickey MD. Stretchable and soft electronics using liquid metals. *Adv Mater* 2017;29:1606425. DOI PubMed

53.   Farrell ZJ, Jacob AR, Truong VK, et al. Compositional design of surface oxides in gallium-indium alloys. *Chem Mater* 2023;35:964-75. DOI

54.   Lu Y, Yu D, Dong H, et al. Dynamic leakage-free liquid metals. *Adv Funct Mater* 2023;33:2210961. DOI

55.   Wang S, Liu C, Liu J, et al. Highly stable liquid metal conductors with superior electrical stability and tough interface bonding for

stretchable electronics. *ACS Appl Mater Interfaces* 2023;15:22291-300. DOI

56. Park CW, Moon YG, Seong H, et al. Photolithography-based patterning of liquid metal interconnects for monolithically integrated stretchable circuits. *ACS Appl Mater Interfaces* 2016;8:15459-65. DOI

57. Afrin S, Haque E, Ren B, Ou JZ. Liquid elementary metals and alloys: synthesis, characterization, properties, and applications. *Appl Mater Today* 2023;31:101746. DOI

58. Zhang ZP, Xia H. Nanoarchitectonics and applications of gallium-based liquid metal micro- and nanoparticles. *ChemNanoMat* 2023;9:e202300078. DOI

59. Xu D, Cao J, Liu F, et al. Liquid metal based nano-composites for printable stretchable electronics. *Sensors* 2022;22:2516. DOI PubMed PMC

60. Segev-Bar M, Haick H. Flexible sensors based on nanoparticles. *ACS Nano* 2013;7:8366-78. DOI PubMed

61. Zheng R, Peng Z, Fu Y, et al. A novel conductive core-shell particle based on liquid metal for fabricating real-time self-repairing flexible circuits. *Adv Funct Mater* 2020;30:1910524. DOI

62. Li H, Qiao R, Davis TP, Tang SY. Biomedical applications of liquid metal nanoparticles: a critical review. *Biosensors* 2020;10:196. DOI PubMed PMC

63. Liu L, Huang H, Wang X, He P, Yang J. Recent advances in printed liquid metals for wearable healthcare sensors: a review. *J Phys D Appl Phys* 2022;55:283002. DOI

64. Zuraiqi K, Zavabeti A, Allioux FM, et al. Liquid metals in catalysis for energy applications. *Joule* 2020;4:2290-321. DOI

65. Yan J, Lu Y, Chen G, Yang M, Gu Z. Advances in liquid metals for biomedical applications. *Chem Soc Rev* 2018;47:2518-33. DOI

66. Xie W, Allioux FM, Ou JZ, Miyako E, Tang SY, Kalantar-Zadeh K. Gallium-based liquid metal particles for therapeutics. *Trends Biotechnol* 2021;39:624-40. DOI PubMed

67. Daeneke T, Khoshmanesh K, Mahmood N, et al. Liquid metals: fundamentals and applications in chemistry. *Chem Soc Rev* 2018;47:4073-111. DOI

68. Lin ZD, Shu SC, Li A, et al. Preparation and mechanical property of graphene-reinforced copper matrix composites. *J Inorg Mater* 2019;34:469-77. DOI

69. Jiang Q, Zhang S, Zhao M. Size-dependent melting point of noble metals. *Mater Chem Phys* 2003;82:225-7. DOI

70. Bulmer JS, Kaniyoor A, Elliott JA. A meta-analysis of conductive and strong carbon nanotube materials. *Adv Mater* 2021;33:2008432. DOI PubMed

71. Ma KQ, Liu J. Nano liquid-metal fluid as ultimate coolant. *Phys Lett A* 2007;361:252-6. DOI

72. Wang Q, Yu Y, Liu J. Preparations, characteristics and applications of the functional liquid metal materials. *Adv Eng Mater* 2018;20:1700781. DOI

73. Tian L, Li Y, Webb RC, et al. Sensors: flexible and stretchable 3ω sensors for thermal characterization of human skin (Adv. Funct. Mater. 26/2017). *Adv Funct Mater* 2017;27:1770159. DOI

74. Singh K, Sharma S, Shriwastava S, Singla P, Gupta M, Tripathi CC. Significance of nano-materials, designs consideration and fabrication techniques on performances of strain sensors - a review. *Mat Sci Semicon Proc* 2021;123:105581. DOI

75. Song M, Daniels KE, Kiani A, Rashid-Nadimi S, Dickey MD. Interfacial tension modulation of liquid metal via electrochemical oxidation. *Adv Intell Syst* 2021;3:2100024. DOI

76. Tang J, Zhao X, Li J, Guo R, Zhou Y, Liu J. Gallium-based liquid metal amalgams: transitional-state metallic mixtures (TransM^{2}ixes) with enhanced and tunable electrical, thermal, and mechanical properties. *ACS Appl Mater Interfaces* 2017;9:35977-87. DOI

77. Guo R, Sun X, Yao S, et al. Semi-liquid-metal-(Ni-EGaIn)-based ultraconformable electronic tattoo. *Adv Mater Technol* 2019;4:1900183. DOI

78. Ren L, Sun S, Casillas-Garcia G, et al. A liquid-metal-based magnetoactive slurry for stimuli-responsive mechanically adaptive electrodes. *Adv Mater* 2018;30:1802595. DOI

79. Li M, Chen D, Deng X, et al. Graded Mxene-doped liquid metal as adhesion interface aiming for conductivity enhancement of hybrid rigid-soft interconnection. *ACS Appl Mater Interfaces* 2023;15:14948-57. DOI

80. Chang H, Zhang P, Guo R, et al. Recoverable liquid metal paste with reversible rheological characteristic for electronics printing. *ACS Appl Mater Interfaces* 2020;12:14125-35. DOI

81. Zhu J, Xu Z, Ha S, et al. Gallium oxide for gas sensor applications: a comprehensive review. *Materials* 2022;15:7339. DOI PubMed PMC

82. Zhang M, Wang X, Huang Z, Rao W. Liquid metal based flexible and implantable biosensors. *Biosensors* 2020;10:170. DOI PubMed PMC

83. Afzal A. β-Ga$_2$O$_3$ nanowires and thin films for metal oxide semiconductor gas sensors: sensing mechanisms and performance enhancement strategies. *J Materiomics* 2019;5:542-57. DOI

84. Fleischer M, Meixner H. Fast gas sensors based on metal oxides which are stable at high temperatures. *Sens Actuators B Chem* 1997;43:1-10. DOI

85. Unser S, Bruzas I, He J, Sagle L. Localized surface plasmon resonance biosensing: current challenges and approaches. *Sensors* 2015;15:15684-716. DOI PubMed PMC

86. Catalán-Gómez S, Redondo-Cubero A, Palomares FJ, Nucciarelli F, Pau JL. Tunable plasmonic resonance of gallium nanoparticles by thermal oxidation at low temperatures. *Nanotechnology* 2017;28:405705. DOI PubMed

87. Knight MW, Coenen T, Yang Y, et al. Gallium plasmonics: deep subwavelength spectroscopic imaging of single and interacting

gallium nanoparticles. *ACS Nano* 2015;9:2049-60.　DOI

88.　Losurdo M, Yi C, Suvorova A, et al. Demonstrating the capability of the high-performance plasmonic gallium-graphene couple. *ACS Nano* 2014;8:3031-41.　DOI

89.　Yang Y, Akozbek N, Kim TH, et al. Ultraviolet-visible plasmonic properties of gallium nanoparticles investigated by variable-angle spectroscopic and mueller matrix ellipsometry. *ACS Photonics* 2014;1:582-9.　DOI

90.　Chen L, Wu M, Jing Q, et al. Gallium/gold composite microspheres fixed on a silicon substrate for surface enhanced Raman scattering. *RSC Adv* 2015;5:67134-40.　DOI

91.　Langer J, Jimenez de Aberasturi D, Aizpurua J, et al. Present and future of surface-enhanced Raman scattering. *ACS Nano* 2020;14:28-117.　DOI

92.　Horák M, Čalkovský V, Mach J, Křápek V, Šikola T. Plasmonic properties of individual gallium nanoparticles. *J Phys Chem Lett* 2023;14:2012-9.　DOI　PubMed　PMC

93.　Gao X, Fan X, Zhang J. Tunable plasmonic gallium nano liquid metal from facile and controllable synthesis. *Mater Horiz* 2021;8:3315-23.　DOI　PubMed

94.　Tang SY, Mitchell DRG, Zhao Q, et al. Phase separation in liquid metal nanoparticles. *Matter* 2019;1:192-204.　DOI

95.　Hou Y, Chang H, Song K, et al. Coloration of liquid-metal soft robots: from silver-white to iridescent. *ACS Appl Mater Interfaces* 2018;10:41627-36.　DOI

96.　Yang Y, Callahan JM, Kim TH, Brown AS, Everitt HO. Ultraviolet nanoplasmonics: a demonstration of surface-enhanced Raman spectroscopy, fluorescence, and photodegradation using gallium nanoparticles. *Nano Lett* 2013;13:2837-41.　DOI　PubMed

97.　Wu PC, Khoury CG, Kim TH, et al. Demonstration of surface-enhanced Raman scattering by tunable, plasmonic gallium nanoparticles. *J Am Chem Soc* 2009;131:12032-3.　DOI　PubMed　PMC

98.　Pau JL, García-marín A, Hernández MJ, Lorenzo E, Piqueras J. Optical biosensing platforms based on Ga-graphene plasmonic structures on Cu, quartz and SiO_2/Si substrates. *Phys Status Solidi B* 2016;253:664-70.　DOI

99.　Cai S, Mayyas M, Saborio MG, et al. Gallium nitride formation in liquid metal sonication. *J Mater Chem C* 2020;8:16593-602.　DOI

100.　Marín AG, García-Mendiola T, Bernabeu CN, et al. Gallium plasmonic nanoparticles for label-free DNA and single nucleotide polymorphism sensing. *Nanoscale* 2016;8:9842-51.　DOI

101.　Chen X, Chen Q, Wu D, et al. Sonochemical and mechanical stirring synthesis of liquid metal nanograss structures for low-cost SERS substrates. *J Raman Spectroscopy* 2018;49:1301-10.　DOI

102.　Alsaif MMYA, Haque F, Alkathiri T, et al. 3D visible-light-driven plasmonic oxide frameworks deviated from liquid metal nanodroplets. *Adv Funct Mater* 2021;31:2106397.　DOI

103.　Li J, Qi C, Lian Z, et al. Cell-capture and release platform based on peptide-aptamer-modified nanowires. *ACS Appl Mater Interfaces* 2016;8:2511-6.　DOI

104.　Liu F, Yu Y, Yi L, Liu J. Liquid metal as reconnection agent for peripheral nerve injury. *Sci Bull* 2016;61:939-47.　DOI

105.　Yi L, Jin C, Wang L, Liu J. Liquid-solid phase transition alloy as reversible and rapid molding bone cement. *Biomaterials* 2014;35:9789-801.　DOI

106.　Chen S, Zhao R, Sun X, Wang H, Li L, Liu J. Toxicity and biocompatibility of liquid metals. *Adv Healthc Mater* 2023;12:2201924.　DOI

107.　Krug HF, Wick P. Nanotoxicology: an interdisciplinary challenge. *Angew Chem Int Ed Engl* 2011;50:1260-78.　DOI　PubMed

108.　Elsaesser A, Howard CV. Toxicology of nanoparticles. *Adv Drug Deliv Rev* 2012;64:129-37.　DOI　PubMed

109.　Kumar VB, Gedanken A, Kimmel G, Porat Z. Ultrasonic cavitation of molten gallium: formation of micro- and nano-spheres. *Ultrason Sonochem* 2014;21:1166-73.　DOI　PubMed

110.　Creighton MA, Yuen MC, Susner MA, Farrell Z, Maruyama B, Tabor CE. Oxidation of gallium-based liquid metal alloys by water. *Langmuir* 2020;36:12933-41.　DOI　PubMed

111.　Adams WT 4th, Nolan MW, Ivanisevic A. Ga ion-enhanced and particle shape-dependent generation of reactive oxygen species in X-ray-irradiated composites. *ACS Omega* 2018;3:5252-9.　DOI　PubMed　PMC

112.　Zhang M, Yao S, Rao W, Liu J. Transformable soft liquid metal micro/nanomaterials. *Mater Sci Eng R Rep* 2019;138:1-35.　DOI

113.　Schedle A, Samorapoompichit P, Rausch-Fan XH, et al. Response of L-929 fibroblasts, human gingival fibroblasts, and human tissue mast cells to various metal cations. *J Dent Res* 1995;74:1513-20.　DOI

114.　Chechetka SA, Yu Y, Zhen X, Pramanik M, Pu K, Miyako E. Light-driven liquid metal nanotransformers for biomedical theranostics. *Nat Commun* 2017;8:15432.　DOI　PubMed　PMC

115.　Tang SY, Qiao R, Lin Y, et al. Functional liquid metal nanoparticles produced by liquid-based nebulization. *Adv Mater Technol* 2019;4:1800420.　DOI

116.　Sun X, Sun M, Liu M, et al. Shape tunable gallium nanorods mediated tumor enhanced ablation through near-infrared photothermal therapy. *Nanoscale* 2019;11:2655-67.　DOI

117.　Lu Y, Hu Q, Lin Y, et al. Transformable liquid-metal nanomedicine. *Nat Commun* 2015;6:10066.　DOI　PubMed　PMC

118.　Kim JH, Kim S, So JH, Kim K, Koo HJ. Cytotoxicity of gallium-indium liquid metal in an aqueous environment. *ACS Appl Mater Interfaces* 2018;10:17448-54.　DOI

119.　Homma T, Ueno T, Sekizawa K, Tanaka A, Hirata M. Interstitial pneumonia developed in a worker dealing with particles containing indium-tin oxide. *J Occup Health* 2003;45:137-9.　DOI

120.　Wang D, Wu Q, Guo R, Lu C, Niu M, Rao W. Magnetic liquid metal loaded nano-in-micro spheres as fully flexible theranostic

agents for SMART embolization. *Nanoscale* 2021;13:8817-36. DOI

121.   Zhang Y, Guo Z, Zhu H, et al. Synthesis of liquid gallium@reduced graphene oxide core-shell nanoparticles with enhanced photoacoustic and photothermal performance. *J Am Chem Soc* 2022;144:6779-90. DOI

122.   Song H, Kim T, Kang S, Jin H, Lee K, Yoon HJ. Ga-based liquid metal micro/nanoparticles: recent advances and applications. *Small* 2020;16:1903391. DOI

123.   Yu F, Xu J, Li H, et al. Ga-In liquid metal nanoparticles prepared by physical vapor deposition. *Prog Nat Sci Mater Int* 2018;28:28-33. DOI

124.   Yarema M, Wörle M, Rossell MD, et al. Monodisperse colloidal gallium nanoparticles: synthesis, low temperature crystallization, surface plasmon resonance and Li-ion storage. *J Am Chem Soc* 2014;136:12422-30. DOI PubMed PMC

125.   Kim S, Kim S, Hong K, Dickey MD, Park S. Liquid-metal-coated magnetic particles toward writable, nonwettable, stretchable circuit boards, and directly assembled liquid metal-elastomer conductors. *ACS Appl Mater Interfaces* 2022;14:37110-9. DOI

126.   Yamaguchi A, Mashima Y, Iyoda T. Reversible size control of liquid-metal nanoparticles under ultrasonication. *Angew Chem Int Ed Engl* 2015;54:12809-13. DOI PubMed

127.   Lu H, Tang SY, Dong Z, et al. Dynamic temperature control system for the optimized production of liquid metal nanoparticles. *ACS Appl Nano Mater* 2020;3:6905-14. DOI

128.   Lin Y, Genzer J, Dickey MD. Attributes, Fabrication, and applications of gallium-based liquid metal particles. *Adv Sci* 2020;7:2000192. DOI PubMed PMC

129.   Tang SY, Qiao R, Yan S, et al. Microfluidic mass production of stabilized and stealthy liquid metal nanoparticles. *Small* 2018;14:1800118. DOI

130.   Lin Y, Genzer J, Li W, Qiao R, Dickey MD, Tang SY. Sonication-enabled rapid production of stable liquid metal nanoparticles grafted with poly(1-octadecene-alt-maleic anhydride) in aqueous solutions. *Nanoscale* 2018;10:19871-8. DOI PubMed

131.   Gan T, Shang W, Handschuh-Wang S, Zhou X. Light-induced shape morphing of liquid metal nanodroplets enabled by polydopamine coating. *Small* 2019;15:1804838. DOI PubMed

132.   Finkenauer LR, Lu Q, Hakem IF, Majidi C, Bockstaller MR. Analysis of the efficiency of surfactant-mediated stabilization reactions of EGaIn nanodroplets. *Langmuir* 2017;33:9703-10. DOI PubMed

133.   Wei Q, Sun M, Wang Z, et al. Surface engineering of liquid metal nanodroplets by attachable diblock copolymers. *ACS Nano* 2020;14:9884-93. DOI

134.   Cossio G, Yu ET. Zeta potential dependent self-assembly for very large area nanosphere lithography. *Nano Lett* 2020;20:5090-6. DOI PubMed

135.   Hu C, Sun Q, He P, et al. Smart adhesive patches of antibacterial performance based on polydopamine-modified Ga liquid metal nanodroplets. *ACS Appl Nano Mater* 2022;5:18349-56. DOI

136.   He B, Liu S, Zhao X, et al. Dialkyl dithiophosphate-functionalized gallium-based liquid-metal nanodroplets as lubricant additives for antiwear and friction reduction. *ACS Appl Nano Mater* 2020;3:10115-22. DOI

137.   Xu D, Hu J, Pan X, Sánchez S, Yan X, Ma X. Enzyme-powered liquid metal nanobots endowed with multiple biomedical functions. *ACS Nano* 2021;15:11543-54. DOI PubMed

138.   Wang P, Xie H, Guo F, et al. Thiadiazole dimer-functionalized liquid metal nanoparticles for anti-corrosion and friction reduction. *ACS Appl Nano Mater* 2023;6:5799-807. DOI

139.   Huang X, Xu T, Shen A, Davis TP, Qiao R, Tang SY. Engineering polymers via understanding the effect of anchoring groups for highly stable liquid metal nanoparticles. *ACS Appl Nano Mater* 2022;5:5959-71. DOI PubMed PMC

140.   Tevis ID, Newcomb LB, Thuo M. Synthesis of liquid core-shell particles and solid patchy multicomponent particles by shearing liquids into complex particles (SLICE). *Langmuir* 2014;30:14308-13. DOI PubMed

141.   Çınar S, Tevis ID, Chen J, Thuo M. Mechanical fracturing of core-shell undercooled metal particles for heat-free soldering. *Sci Rep* 2016;6:21864. DOI PubMed PMC

142.   Li X, Wang Z, Dong G. Preparation of nanoscale liquid metal droplet wrapped with chitosan and its tribological properties as water-based lubricant additive. *Tribol Int* 2020;148:106349. DOI

143.   Hafiz SS, Labadini D, Riddell R, et al. Surfaces and interfaces of liquid metal core-shell nanoparticles under the microscope. *Part Part Syst Charact* 2020;37:1900469. DOI PubMed PMC

144.   Cutinho J, Chang BS, Oyola-Reynoso S, et al. Autonomous thermal-oxidative composition inversion and texture tuning of liquid metal surfaces. *ACS Nano* 2018;12:4744-53. DOI

145.   Hoang TT, Phan PT, Thai MT, et al. Magnetically engineered conductivity of soft liquid metal composites for robotic, wearable electronic, and medical applications. *Adv Intell Syst* 2022;4:2270059. DOI

146.   Yu L, Qi X, Liu Y, Chen L, Li X, Xia Y. Transportable, endurable, and recoverable liquid metal powders with mechanical sintering conductivity for flexible electronics and electromagnetic interference shielding. *ACS Appl Mater Interfaces* 2022;14:48150-60. DOI

147.   Zeng H, Du XW, Singh SC, et al. Nanomaterials via laser ablation/irradiation in liquid: a review. *Adv Funct Mater* 2012;22:1333-53. DOI

148.   Im HG, Jin J, Ko JH, Lee J, Lee JY, Bae BS. Flexible transparent conducting composite films using a monolithically embedded AgNW electrode with robust performance stability. *Nanoscale* 2014;6:711-5. DOI

149.   Zeng X, He P, Hu M, et al. Copper inks for printed electronics: a review. *Nanoscale* 2022;14:16003-32. DOI

150.   Yu J, Xia J, Guan X, et al. Self-healing liquid metal confined in carbon nanofibers/carbon nanotubes paper as a free-standing anode

for flexible lithium-ion batteries. *Electrochimica Acta* 2022;425:140721. DOI

151. Lou Y, Liu H, Zhang J. Liquid metals in plastics for super-toughness and high-performance force sensors. *Chem Eng J* 2020;399:125732. DOI

152. Xu C, Zheng Z, Lin M, et al. Strengthened, antibacterial, and conductive flexible film for humidity and strain sensors. *ACS Appl Mater Interfaces* 2020;12:35482-92. DOI

153. Lei D, Zhang H, Liu N, et al. Tensible and flexible high-sensitive spandex fiber strain sensor enhanced by carbon nanotubes/Ag nanoparticles. *Nanotechnology* 2021;32:505509. DOI

154. Xu S, Zong Y, Ma J, Liu L. A multifunctional skin-like sensor based on liquid metal activated gelatin organohydrogel. *Adv Mater Interfaces* 2022;9:2201212. DOI

155. Huang Y, Yang F, Liu S, Wang R, Guo J, Ma X. Liquid metal-based epidermal flexible sensor for wireless breath monitoring and diagnosis enabled by highly sensitive SnS_2 nanosheets. *Research* 2021;2021:9847285. DOI

156. Chi Y, Han J, Zheng J, et al. Insights into the interfacial contact and charge transport of gas-sensing liquid metal marbles. *ACS Appl Mater Interfaces* 2022;14:30112-23. DOI

157. Schlingman K, D'amaral GM, Carmichael RS, Carmichael TB. Intrinsically conductive liquid metal-elastomer composites for stretchable and flexible electronics. *Adv Mater Technol* 2023;8:2200374. DOI

158. Lopes PA, Fernandes DF, Silva AF, et al. Bi-phasic Ag-In-Ga-embedded elastomer inks for digitally printed, ultra-stretchable, multi-layer electronics. *ACS Appl Mater Interfaces* 2021;13:14552-61. DOI

159. Pan X, Guo D, He H. Novel conductive polymer composites based on CNTs/CNFs bridged liquid metal. *J Phys D Appl Phys* 2021;54:085401. DOI

160. Lu Y, Lin Y, Chen Z, et al. Enhanced endosomal escape by light-fueled liquid-metal transformer. *Nano Lett* 2017;17:2138-45. DOI

161. Xu J, Wang Z, You J, et al. Polymerization of moldable self-healing hydrogel with liquid metal nanodroplets for flexible strain-sensing devices. *Chem Eng J* 2020;392:123788. DOI

162. Li Y, Feng S, Cao S, Zhang J, Kong D. Printable liquid metal microparticle ink for ultrastretchable electronics. *ACS Appl Mater Interfaces* 2020;12:50852-9. DOI

163. Chiu SH, Baharfar M, Chi Y, et al. Exploring electrical conductivity of thiolated micro- and nanoparticles of gallium. *Adv Intell Syst* 2023;5:2200364. DOI

164. Hou Y, Lu C, Dou M, et al. Soft liquid metal nanoparticles achieve reduced crystal nucleation and ultrarapid rewarming for human bone marrow stromal cell and blood vessel cryopreservation. *Acta Biomater* 2020;102:403-15. DOI

165. Idrus-Saidi SA, Tang J, Yang J, et al. Liquid metal-based route for synthesizing and tuning gas-sensing elements. *ACS Sens* 2020;5:1177-89. DOI

166. Hoshyargar F, Khan H, Kalantar-zadeh K, O'Mullane AP. Generation of catalytically active materials from a liquid metal precursor. *Chem Commun* 2015;51:14026-9. DOI PubMed

167. Liang S, Wang C, Li F, Song G. Supported Cu/W/Mo/Ni - liquid metal catalyst with core-shell structure for photocatalytic degradation. *Catalysts* 2021;11:1419. DOI

168. Zhang W, Ou JZ, Tang SY, et al. Liquid metal/metal oxide frameworks. *Adv Funct Mater* 2014;24:3799-807. DOI

169. Sivan V, Tang SY, O'Mullane AP, et al. Liquid metal marbles. *Adv Funct Materials* 2013;23:144-52. DOI

170. Nucciarelli F, Bravo I, Vázquez L, Lorenzo E, Pau JL. Gallium nanoparticles colloids synthesis for UV bio-optical sensors. *Optical Sensors* 2017;10231:407-13. DOI

171. Boley JW, White EL, Kramer RK. Mechanically sintered gallium-indium nanoparticles. *Adv Mater* 2015;27:2355-60. DOI PubMed

172. Zhang P, Wang Q, Guo R, et al. Self-assembled ultrathin film of CNC/PVA-liquid metal composite as a multifunctional Janus material. *Mater Horiz* 2019;6:1643-53. DOI

173. Wu P, Zhou L, Lv S, Fu J, He Y. Self-sintering liquid metal ink with LAPONITE® for flexible electronics. *J Mater Chem C* 2021;9:3070-80. DOI

174. Li X, Li M, Zong L, et al. Liquid metal droplets wrapped with polysaccharide microgel as biocompatible aqueous ink for flexible conductive devices. *Adv Funct Mater* 2018;28:1804197. DOI

175. Liu Y, Wang Q, Bi S, Zhang W, Zhou H, Jiang X. Water-processable liquid metal nanoparticles by single-step polymer encapsulation. *Nanoscale* 2020;12:13731-41. DOI

176. Liu S, Yuen MC, White EL, et al. Laser sintering of liquid metal nanoparticles for scalable manufacturing of soft and flexible electronics. *ACS Appl Mater Interfaces* 2018;10:28232-41. DOI

177. Liu S, Kim SY, Henry KE, Shah DS, Kramer-Bottiglio R. Printed and laser-activated liquid metal-elastomer conductors enabled by ethanol/PDMS/liquid metal double emulsions. *ACS Appl Mater Interfaces* 2021;13:28729-36. DOI PubMed

178. Zheng L, Zhu M, Wu B, Li Z, Sun S, Wu P. Conductance-stable liquid metal sheath-core microfibers for stretchy smart fabrics and self-powered sensing. *Sci Adv* 2021;7:eabg4041. DOI PubMed PMC

179. Ning C, Wei C, Sheng F, et al. Scalable one-step wet-spinning of triboelectric fibers for large-area power and sensing textiles. *Nano Res* 2023;16:7518-26. DOI

180. Zhang M, Li G, Huang L, et al. Versatile fabrication of liquid metal nano-ink based flexible electronic devices. *Appl Mater Today* 2021;22:100903. DOI

181. Zhang Q, Gao Y, Liu J. Atomized spraying of liquid metal droplets on desired substrate surfaces as a generalized way for ubiquitous printed electronics. *Appl Phys A* 2014;116:1091-7. DOI

182. Li BM, Reese BL, Ingram K, et al. Textile-integrated liquid metal electrodes for electrophysiological monitoring. *Adv Healthc Mater* 2022;11:2200745. DOI

183. Hu Y, Hao X, Chen G, Bian J, Li M, Peng F. Self-standing, photothermal-actuating, and motion-monitoring janus films one-pot synthesized by green carboxymethyl glucomannan/liquid metal nanoinks. *ACS Appl Mater Interfaces* 2022;14:23717-25. DOI

184. Niu Y, Tian G, Liang C, et al. Thermal-sinterable EGaIn nanoparticle inks for highly deformable bioelectrode arrays. *Adv Healthc Mater* 2022;12:2202531. DOI

185. Park K, Pyeon J, Jeong SH, Yoon YJ, Kim H. Avalanche coalescence of liquid metal particles for uniform flexible and stretchable electrodes. *Adv Mater Interfaces* 2022;9:2201693. DOI

186. Lee GH, Woo H, Yoon C, et al. A personalized electronic tattoo for healthcare realized by on-the-spot assembly of an intrinsically conductive and durable liquid-metal composite (Adv. Mater. 32/2022). *Adv Mater* 2022;34:2270236. DOI

187. Liu Y, Yang L, Chen Q, et al. Deposition of vertically aligned Ag/Ag$_2$S nanoflakes on EGaIn particles for humidity sensing. *Chemistry* 2022;28:e202200298. DOI

188. Yang Y, Han J, Huang J, et al. Stretchable energy-harvesting tactile interactive interface with liquid-metal-nanoparticle-based electrodes. *Adv Funct Mater* 2020;30:1909652. DOI

189. Zhang Z, Tang L, Chen C, et al. Liquid metal-created macroporous composite hydrogels with self-healing ability and multiple sensations as artificial flexible sensors. *J Mater Chem A* 2021;9:875-83. DOI

190. Xu Y, Rothe R, Voigt D, et al. Convergent synthesis of diversified reversible network leads to liquid metal-containing conductive hydrogel adhesives. *Nat Commun* 2021;12:2407. DOI PubMed PMC

191. Chen B, Liu G, Wu M, et al. Liquid metal-based organohydrogels for wearable flexible electronics. *Adv Mater Technol* 2023;8:2201919. DOI

192. Zhou L, Li Y, Xiao J, et al. Liquid metal-doped conductive hydrogel for construction of multifunctional sensors. *Anal Chem* 2023;95:3811-20. DOI

193. Dong Y, Wang C, Hu Z, et al. A sandwich-structure, low-temperature sensitive and recyclable liquid metal organic hydrogel for a wearable strain sensor. *J Appl Polymer Sci* 2022;139:e53174. DOI

194. Liao M, Liao H, Ye J, Wan P, Zhang L. Polyvinyl alcohol-stabilized liquid metal hydrogel for wearable transient epidermal sensors. *ACS Appl Mater Interfaces* 2019;11:47358-64. DOI PubMed

195. Cheng J, Shang J, Yang S, Dou J, Shi X, Jiang X. Wet-adhesive elastomer for liquid metal-based conformal epidermal electronics. *Adv Funct Mater* 2022;32:2200444. DOI

196. Zhao B, Bai Z, Lv H, et al. Self-healing liquid metal magnetic hydrogels for smart feedback sensors and high-performance electromagnetic shielding. *Nanomicro Lett* 2023;15:79. DOI PubMed PMC

197. Wang M, Feng X, Wang X, Hu S, Zhang C, Qi H. Facile gelation of a fully polymeric conductive hydrogel activated by liquid metal nanoparticles. *J Mater Chem A* 2021;9:24539-47. DOI

198. Feng X, Wang C, Shang S, et al. Self-healing, EMI shielding, and antibacterial properties of recyclable cellulose liquid metal hydrogel sensor. *Carbohydr Polym* 2023;311:120786. DOI

199. Liu S, Guo Q, Wang X, Li G, Ma X, Xu Z. Fabrication of liquid metal loaded polycaprolactone conductive film for biocompatible and flexible electronics. *Biosens Bioelectron X* 2022;11:100182. DOI

200. Chen B, Cao Y, Li Q, et al. Liquid metal-tailored gluten network for protein-based e-skin. *Nat Commun* 2022;13:1206. DOI PubMed PMC

201. Chen B, Wu M, Fang S, et al. Liquid metal-tailored PEDOT:PSS for noncontact flexible electronics with high spatial resolution. *ACS Nano* 2022;16:19305-18. DOI

202. Lee GH, Lee YR, Kim H, et al. Rapid meniscus-guided printing of stable semi-solid-state liquid metal microgranular-particle for soft electronics. *Nat Commun* 2022;13:2643. DOI PubMed PMC

203. Cao J, Liang F, Li H, et al. Ultra-robust stretchable electrode for e-skin: In situ assembly using a nanofiber scaffold and liquid metal to mimic water-to-net interaction. *InfoMat* 2022;4:e12302. DOI

204. Zhang C, Allioux FM, Rahim MA, et al. Nucleation and growth of polyaniline nanofibers onto liquid metal nanoparticles. *Chem Mater* 2020;32:4808-19. DOI

205. Sippel JM, Holden WE, Tilles SA, et al. Exhaled nitric oxide levels correlate with measures of disease control in asthma. *J Allergy Clin Immunol* 2000;106:645-50. DOI

206. Yeung DKW, Griffith JF, Li AFW, Ma HT, Yuan J. Air pressure-induced susceptibility changes in vascular reactivity studies using BOLD MRI. *J Magn Reson Imaging* 2013;38:976-80. DOI PubMed

207. Wang C, Li J, Fang Z, et al. Temperature-stress bimodal sensing conductive hydrogel-liquid metal by facile synthesis for smart wearable sensor. *Macromol Rapid Commun* 2022;43:2100543. DOI

208. Kim S, Lee J. Indentation and temperature response of liquid metal/hydrogel composites. *J Ind Eng Chem* 2022;110:225-33. DOI

209. Gutiérrez Y, Losurdo M, García-fernández P, et al. Gallium polymorphs: phase-dependent plasmonics. *Adv Opt Mater* 2019;7:1900307. DOI

210. Losurdo M, Suvorova A, Rubanov S, Hingerl K, Brown AS. Thermally stable coexistence of liquid and solid phases in gallium nanoparticles. *Nat Mater* 2016;15:995-1002. DOI PubMed

211. Li X, Zhu P, Zhang S, et al. A self-supporting, conductor-exposing, stretchable, ultrathin, and recyclable kirigami-structured liquid metal paper for multifunctional e-skin. *ACS Nano* 2022;16:5909-19. DOI

212. Wang S, Zhao X, Luo J, Zhuang L, Zou D. Liquid metal (LM) and its composites in thermal management. *Compos Part A Appl Sci Manuf* 2022;163:107216. DOI

213. Reineck P, Lin Y, Gibson BC, Dickey MD, Greentree AD, Maksymov IS. UV plasmonic properties of colloidal liquid-metal eutectic gallium-indium alloy nanoparticles. *Sci Rep* 2019;9:5345. DOI PubMed PMC

214. Qu X, Xue J, Liu Y, Rao W, Liu Z, Li Z. Fingerprint-shaped triboelectric tactile sensor. *Nano Energy* 2022;98:107324. DOI